7-26-2023

Differential Expression of Genes Involved in the Chronic Response to Intracortical Microelectrodes

Sydney S. Song
Case Western Reserve University, sss176@case.edu

Lindsey N. Druschel
Case Western Reserve University, lnd24@case.edu

E. Ricky Chan
Case Western Reserve University, erc6@case.edu

Jeffrey R. Capadona
Case Western Reserve University, jrc35@case.edu

Author(s) ORCID Identifier:

Sydney S. Song

Lindsey N. Druschel

Jeffrey R. Capadona

Recommended Citation

Sydney Song, Lindsey N. Druschel, E. Ricky Chan, Jeffrey R. Capadona. Differential expression of genes involved in the chronic response to intracortical microelectrodes. Acta Biomaterialia, Volume 169, 2023, Pages 348-362. https://doi.org/10.1016/j.actbio.2023.07.038

Acta Biomaterialia 169 (2023) 348–362

Contents lists available at ScienceDirect

Acta Biomaterialia

journal homepage: www.elsevier.com/locate/actbio

Full length article

Differential expression of genes involved in the chronic response to intracortical microelectrodes

Sydney Song[a,b], Lindsey N. Druschel[a,b], E. Ricky Chan[c], Jeffrey R. Capadona[a,b,*]

[a] Department of Biomedical Engineering, Case Western Reserve University, Cleveland, OH 44106, United States
[b] Advanced Platform Technology Center, Louis Stokes Cleveland Veterans Affairs Medical Center, Cleveland, OH 44106, United States
[c] Cleveland Institute for Computational Biology, Case Western Reserve University, Cleveland, OH 44106, United States

ARTICLE INFO

Article history:
Received 27 January 2023
Revised 13 July 2023
Accepted 23 July 2023
Available online 26 July 2023

Keywords:
Microelectrode
Inflammation
Cytokine
Chronic

ABSTRACT

Brain-Machine Interface systems (BMIs) are clinically valuable devices that can provide functional restoration for patients with spinal cord injury or improved integration for patients requiring prostheses. Intracortical microelectrodes can record neuronal action potentials at a resolution necessary for precisely controlling BMIs. However, intracortical microelectrodes have a demonstrated history of progressive decline in the recording performance with time, inhibiting their usefulness. One major contributor to decreased performance is the neuroinflammatory response to the implanted microelectrodes. The neuroinflammatory response can lead to neurodegeneration and the formation of a glial scar at the implant site. Historically, histological imaging of relatively few known cellular and protein markers has characterized the neuroinflammatory response to implanted microelectrode arrays. However, neuroinflammation requires many molecular players to coordinate the response - meaning traditional methods could result in an incomplete understanding. Taking advantage of recent advancements in tools to characterize the relative or absolute DNA/RNA expression levels, a few groups have begun to explore gene expression at the microelectrode-tissue interface. We have utilized a custom panel of ~813 neuroinflammatory-specific genes developed with NanoString for bulk tissue analysis at the microelectrode-tissue interface. Our previous studies characterized the acute innate immune response to intracortical microelectrodes. Here we investigated the gene expression at the microelectrode-tissue interface in wild-type (WT) mice chronically implanted with nonfunctioning probes. We found 28 differentially expressed genes at chronic time points (4WK, 8WK, and 16WK), many in the complement and extracellular matrix system. Further, the expression levels were relatively stable over time. Genes identified here represent chronic molecular players at the microelectrode implant sites and potential therapeutic targets for the long-term integration of microelectrodes.

Statement of significance

Intracortical microelectrodes can record neuronal action potentials at a resolution necessary for the precise control of Brain-Machine Interface systems (BMIs). However, intracortical microelectrodes have a demonstrated history of progressive declines in the recording performance with time, inhibiting their usefulness. One major contributor to the decline in these devices is the neuroinflammatory response against the implanted microelectrodes. Historically, neuroinflammation to implanted microelectrode arrays has been characterized by histological imaging of relatively few known cellular and protein markers. Few studies have begun to develop a more in-depth understanding of the molecular pathways facilitating device-mediated neuroinflammation. Here, we are among the first to identify genetic pathways that could represent targets to improve the host response to intracortical microelectrodes, and ultimately device performance.

* Corresponding author at: Case Western Reserve University, 2071 Martin Luther King Jr. Drive, Cleveland, OH, United States.
E-mail address: jrc35@case.edu (J.R. Capadona).

https://doi.org/10.1016/j.actbio.2023.07.038
1742-7061/Published by Elsevier Ltd on behalf of Acta Materialia Inc. This is an open access article under the CC BY-NC-ND license
(http://creativecommons.org/licenses/by-nc-nd/4.0/)

1. Introduction

Intracortical Microelectrode Arrays (MEAs) implanted in the cortex of the brain have been widely used to develop brain-machine interface technologies (BMIs) because of their ability to record high-resolution neural activity [1]. For example, the recorded neural activity can be used to restore lost functions in paralyzed and injured individuals [2–8]. Many basic neuroscience research studies and clinical applications are under consideration and development [9–21]. Unfortunately, implantation of MEAs into the brain breaches the blood-brain barrier, damages brain tissue, and initiates a neuroinflammatory cascade [22–25]. The neuroinflammatory response to MEAs exists if the device remains implanted and significantly contributes to the decline in the quantity and quality of detectable neural activity [14].

Over the last several decades, one primary focus in improving the clinical relevance of BMIs is inhibiting the neuroinflammatory response. Many approaches have been pursued, including (but not limited to): minimizing the trauma associated with device implantation [26,27], minimizing the device/tissue stiffness mismatch [28–36], and reducing oxidative stress/damage [30,37–44]. Inflammatory responses have been broadly targeted either with glucocorticoids such as dexamethasone or anti-inflammatory antibiotics such as Minocycline, or more specifically by altering the quantity or function of specific molecules such as laminin, melatonin, flavopiridol, caspase-1, and CD14 [45–52]. Alternatively, ECM-derived compounds that stimulate neuronal growth have also reduced the inflammatory response against microelectrodes [53,54]. While broadly targeting anti-inflammatory molecules has improved the recording quality in mice [45,46], long-term immune modulation may lead to severe side effects [55–58]. Approaches to reduce microelectrode-induced inflammation should consider that a significant target population of BMI systems is also present with decreased immune function and increased risk for infection [59–62]. Therefore, approaches targeting specific molecules or parts of the inflammatory system may reduce or circumvent some of the side effects of non-specific therapy.

The neuroinflammatory response and subsequent neurodegenerative response are complex. Until recently, the investigation of responsible inflammatory mediators was constrained to only a handful at a time [63]. Utilizing advancements such as developing highly parallel gene expression assays, several groups have begun investigating the expressions of sizable gene sets at the microelectrode-tissue interface [43,64–66]. We started our investigation of gene expression levels associated with the neuroinflammatory response to MEAs focused on a small number of genes concentrated on a specific aspect of the neurodegenerative process – oxidative stress [67]. We then expanded our toolset and characterized the expression of nearly 800 genes at the microelectrode-tissue interface of WT mice at acute time points of up to 2 weeks post-surgery [63,68]. Our initial efforts identified hundreds of differentially expressed genes at acute time points (6H, 24H, 72H, and 2WKs post-surgery). Upregulation of some genes began as early as 6H post-implantation, while others started between 72H to 2WKs post-surgery. As an example, the cluster of differentiation 14 (*Cd14*) gene, a molecule in the Pathogen Recognition Receptor (PRR) pathway, was upregulated in response to microelectrode implantation at several time points post-surgery [63]. In corroboration of these findings, it is essential to recall that $Cd14^{-/-}$ mice exhibited improved microelectrode recording quality at acute time points [47]. Further, we found differential gene expression for cytokine, chemokine, and complement pathways at acute time points to be similar in $Cd14^{-/-}$ and WT. However, the time to peak expression level was delayed in $Cd14^{-/-}$ mice compared to WT mice (72 hours in $Cd14^{-/-}$ mice vs. 24 hours in WT mice) [68]. Thus, based on our studies as well as that of other labs, cytokine, chemokine, and complement pathways have been identified as central pathways in the neuroinflammatory response against microelectrodes, with many members differentially expressed at acute time points post-surgery [43,63–65,68].

Recently, the Purcell and Hofmann groups have begun to explore the transcriptomic analysis of the microelectrode interface [65,66]. Some technologies, such as 10x genomics, allow for in-depth coverage of gene expression with spatial resolution - representing great promise for improving our understanding of the microelectrode-tissue interface. However, such techniques can quickly become cost-prohibitive and more challenging to scale up for larger sample sets. Therefore, we have again utilized a custom gene set of ~800 neuroinflammatory-specific genes developed with NanoString for bulk analysis of the tissue adjacent to the microelectrode-tissue interface. Many of the molecular players identified in previous acute-time point focused studies are early responders that show decreased upregulation by 2WK post-surgery, with most genes showing peak upregulation 24 – 72 hours post-surgery. Therefore, we hypothesized that the profile of molecular players at chronic time points post-surgery would differentiate from that of acute time points. Here, we expected fewer upregulated genes in the neuroinflammatory pathway, with later-stage upregulation of anti-inflammatory and wound-healing molecules. Here, we will report our findings for WT mice implanted with MEAs for 4WK, 8WK, and 16WK post-surgery.

2. Materials and methods

The materials and methods used in this paper were previously described. Refer to Bedell et al. [63] and Song et al. [68] for more details. Briefly:

2.1. Animals

We performed all animal care, handling, and procedures in compliance with a protocol approved by the Institutional Animal Care and Use Committee (IACUC) at Case Western Reserve University. Twenty male C57BL/6J mice (Jackson Laboratory Strain #003724) were obtained from Jackson laboratory between 7 – 10 weeks of age and housed for 1 – 4 weeks before surgery was performed in a class II sterile hood using microisolator techniques. Mice were housed at 3-5 per cage before surgery and 1 per cage post-surgery to prevent physical damage to the microelectrodes or implant sites. The surgeon was blinded from the survival duration group (4WK, 8WK, or 16WK). An additional set of control mice (non-surgical control mice) did not receive any surgical procedures. The 20 mice were divided equally among the three experimental and one control group for an N = 5 per group.

2.2. Nonfunctional “dummy” microelectrode probes

Nonfunctional “dummy” silicon probes were received from the Pancrazio and Cogan Laboratories at the University of Texas at Dallas [69,70]. Dummy probes mirrored the physical dimensions of single-shank Michigan-style microelectrode arrays. Probes were 15 µm thick, 123 µm wide along the widest parts of the shank, and 2 mm long from base to tip. Before implantation, dummy probes were washed by soaking in 95% ethanol solution three times for 5 minutes each and sterilized by cold ethylene oxide gas following established protocols [71–73].

2.3. Surgical procedure

Before surgery, each mouse was anesthetized with isoflurane (3% in 1.0 L/min O_2 for induction, 2% in 1.0 L/min O_2 for main-

tenance) and placed in a stereotactic frame. Once anesthetized, Meloxicam (2 mg/kg) and Buprenorphine (0.05 mg/kg) were given subcutaneously as a systemic analgesic. While Meloxicam can inhibit neuroinflammation, the effects are short-lived, with a half-life of ~20 hours, and is thus not expected to impact the chronic neuroinflammatory response studied here [74]. The surgical site was prepared by first shaving the hair, then treated with local analgesic (0.2 ml of 0.25% Marcaine subcutaneously), and sterilized with alternating betadine and isopropanol swabs. A ~1 cm midline incision exposed the skull. Then, we cleaned the tissue adhered to the skull with a hydrogen peroxide swab. Four craniotomies were drilled following established protocols to minimize damage to the blood-brain barrier [26,75], using a 0.45 mm dental drill bit: 1.5 mm lateral and 1.0 mm anterior and posterior to the bregma. Nonfunctional dummy probes were manually inserted into each hole to approximately 1.0-1.5 mm in depth at the speed of ~ 2 – 3 mm/s. Kwik-Sil was used to seal the craniotomies, and dental cement (Flow-It) tethered the dummy probes to the skull. The skin was closed with a 5-0 monofilament polypropylene suture. Meloxicam (2 mg/kg, SQ) and Buprenorphine (0.05 mg/kg, SQ) were administered for three days post-operatively for pain management. Pre-surgical naïve sham mice were used as controls (Non-Surgical Control, or NSCTR) for later comparison.

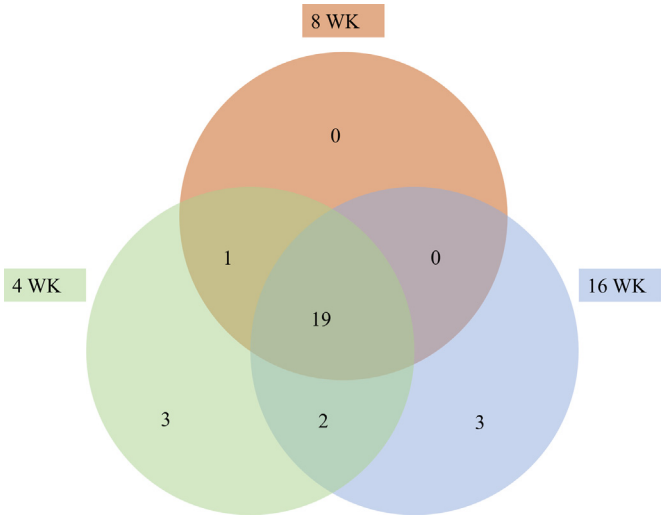

Fig. 1. Gene expression at the microelectrode-tissue interface. Venn Diagram indicating the number of genes differentially expressed for each time point examined, compared to the NSCTR mice at chronic time points. Overlapping regions of the Venn diagrams were used to show an overlap of differentially expressed genes at 4WK, 8WK, and 16WK post-surgery compared to naïve sham control mice, $P_{adj} < 0.05$ and Log2FoldChange > 1 or < -1.

2.4. Tissue extraction

Mice were anesthetized with a ketamine-xylazine cocktail (100mg/Kg and 10mg/Kg, respectively) to a deep surgical plane for euthanasia via cardiac perfusions with cold 1X phosphate-buffered saline (PBS). Perfusions required 50-100 mL PBS for the exudate to run clear. To prevent excessive RNA degradation, we immediately extracted mouse brains. Probes were explanted before flash freezing of the brains in optimal cutting temperature compound (OCT). We stored frozen brains at -80°C until further processing. Cortical brain tissues surrounding the neural probes were cryo-sectioned into 150 µm thick frozen slices. We collected six to seven 150 µm thick sections for this study and stored eight to ten 5 µm thick sections randomly distributed between thicker sections for future studies.

2.5. RNA isolation

Extracted brain tissue was homogenized by placing collected samples directly into 2.0 mL homogenization microtubes prefilled with 1.5 mm zirconium beads (Benchmark scientific D1032-15) and 1 mL Qiazol (RNA extraction lysate) [63]. The microtubes were then loaded onto a Bead Bug Homogenizer (Benchmark Scientific D1030) and shaken at 4000 rpm for 1 min.

The RNA was extracted and purified from the homogenized tissue using RNeasy® Plus Universal Mini Kit (Qiagen 73404) at the Gene Expression and Genotyping Facility at Case Western Reserve University. RNA quality and quantity were determined using Nanodrop. We concentrated samples with low concentration with a Speedvac. Isolated RNA was stored at -80°C for up to two months before sequencing.

2.6. Gene expression assay

We used a barcode technology developed by NanoString Technologies (Seattle, WA) to determine gene expression by counting individual genes. We hybridized RNA (~100 ng per sample) with a codeset containing capture probes and reporter probes genes of interest. Here, we utilized a codeset containing 826 genes; 758 were target genes from the nCounter® Mouse Neuroinflammation Panel, with 13 additional housekeeping genes and 55 custom genes of interest (Table 1). Negative controls and positive controls were spiked in. Samples were incubated at 65°C for 16 hours, loaded onto cartridges, and processed with nCounter® Max Analyzer. Measurements were taken at 280 Field-of-View per sample, and the relative number of each gene was determined from absolute counts of fluorescent barcode reporters using the nCounter® MAX Analyzer.

2.7. Statistical analysis

2.7.1. Normalization

Normalization was performed following established protocols utilizing nSolver, provided by NanoString Technologies [68]. Each sample's raw counts were normalized to raw spiked-in positive controls and housekeeping gene controls. In this study, we utilized ten housekeeping genes for normalization (Table 1), while genes with counts below 25 in 85% of the samples were excluded from the analysis. Here, 242 genes were removed from analysis based on the exclusion criteria leaving 571 genes for further analysis (Fig. 1).

2.7.2. Comparison of gene expression at each post-surgical time point to naïve non-surgical control

As previously described, changes in gene expression were presented as a ratio between each time point (4WK, 8WK, and 16WK) to the single group of pre-surgical naïve sham mice (non-surgical control mice or NSCTR) [68] in a pairwise fashion. Bilateral implantation of the mice prevented contralateral tissue from being used as a non-surgical control. The ratio was then plotted on a Log2 scale (henceforth called Log2FoldChange). The standard error of the mean was calculated and plotted for each pair. An unpaired T-test with Benjamini-Yekutieli False-Discovery-Rate Correction is used to determine statistical significance. Significance is set at p-value adjusted (P_{adj}) < 0.05.

Genes with altered expression at threshold Log2FoldChange > 1 or < -1 (i.e., 2-fold increase or decrease in expression), P_{adj} <0.05, at overlapping time points, were counted and visualized with a Venn diagram. Volcano plot and pathway analysis are generated using the Advanced Analysis Plug-in of nSolver. Bar graphs of altered expression of specific genes are generated using Matlab.

Table 1
Comprehensive table for neuroinflammatory genes of interest utilized in this study. Here we list the 826 genes examined in the current study. Genes from the nCounter® Mouse Neuroinflammation Panel (shown in black), the 55 custom genes of interest are in blue, and 13 housekeeping genes are in red.

Abcc3	Bok	Cd8a	Ddb2	Foxp3	Igsf10	Klr3dl2	Mmp14	Parp1	Rad51c	Smarca4	Tnfrsf13c
Abcc8	Bola2	Cd8b1	Ddx58	Fpr1	Igsf6	Kit	Mmp16	Parp2	Rad9a	Smarca5	Tnfrsf17
Abl1	Braf	Cdc25a	Dicer1	Fscn1	Ikbkb	Klrb1	Mmp19	Pcna	Rag1	Smarcd1	Tnfrsf1a
Adamts13	Brca1	Cdc7	Dlg1	Fyn	Ikbke	Klrd1	Mmp2	Pdpn	Rala	Smc1a	Tnfrsf1b
Adamts16	Brd2	Cdk20	Dlg4	Gadd45a	Ikbkg	Klrk1	Mmp24	Pecam1	Ralb	Snca	Tnfrsf25
Ago4	Brd3	Cdkn1a	Dlx1	Gadd45g	Il10	Kmt2a	Mmp9	Pex14	Rapgef3	Socs3	Tnfrsf4
Agt	Brd4	Cdkn1c	Dlx2	Gal3st1	Il10rb	Kmt2c	Mobp	Pik3ca	Rb1cc1	Sod1	Tnfsf10
Al464131	Btk	Ceacam3	Dna2	Gba	Il15ra	Lacc1	Mag	Pik3cb	Rbfox3	Sod2	Tnfsf12
Aim2	C1qa	Cfb	Dnmt1	Gbp2	Il1a	Lag3	Mok	Pik3cd	Rela	Sod3	Tnfsf13b
Ak1	C1qb	Cfh	Dnmt3a	Gclc	Il1b	Lair1	Mpeg1	Pik3cg	Relb	Sox10	Tnfsf4
Akt1	C1qc	Cfi	Dnmt3b	Gdpd2	Il1f5	Lama1	Mpg	Pik3r1	Reln	Sox4	Tnfsf8
Akt2	C3	Cflar	Dock1	Gfap	Il1r1	Lamb1	Mr1	Pik3r2	Reserved	Sox9	Top2a
Aldh1l1	C3ar1	Ch25h	Dock2	Gja1	Il1r2	Lamb2	Mre11a	Pik3r5	Rgl1	Sphk1	Topbp1
Ambra1	C4a	Chek1	Dot1l	Gjb1	Il1rap	Lamp1	Ms4a1	Pilra	Rhoa	Spib	Tpd52
Amigo2	C4bp	Chek2	Dst	Gna15	Il1rl2	Lamp2	Ms4a2	Pilrb1	Ripk1	Spint1	Tpsb2
Anapc15	C5ar1	Chn2	Duoxa1	Gpr183	Il1rn	Lcn2	Ms4a4a	Pink1	Ripk2	Spp1	Tradd
Anxa1	C6	Chst8	Dusp7	Gpr34	Il21r	Ldha	Msh2	Pla2g4a	Rnf8	Sqstm1	Traf1
Apc	C7	Chuk	E2f1	Gpr62	Il2rg	Ldlrad3	Msn	Pla2g5	Robo3	Srgn	Traf2
Apex1	C9	Cidea	Eed	Gpr84	Il3	Lfng	Msr1	Plcg2	Rpa1	Srxn1	Traf3
Apoe	Cables1	Cideb	Eef2k	Grap	Il3ra	Lgmn	Mvp	Pld1	Rpl28	St3gal6	Traf6
App	Calcoco2	Cks1b	Egfr	Gria1	Il6	Lig1	Myc	Pld2	Rpl29	St8sia6	Trat1
Aqp4	Calr	Clcf1	Egr1	Gria2	Il6ra	Lilrb4a	Myct1	Plekhb1	Rpl36al	Stat1	Trem1
Arc	Camk4	Cldn5	Ehd2	Gria4	iNos	Lingo1	Myd88	Plekhm1	Rpl9	Steap4	Trem2
Arg1	Casp1	Clec4e	Ehmt2	Grin2a	Inpp5d	Lmna	Myrf	Pllp	Rps10	Stmn1	Trem3
Arhgap24	Casp2	Clec7a	Eif1	Grin2b	Iqsec1	Lmnb1	Nbn	Plp1	Rps2	Stx18	Trim47
Arid1a	Casp3	Clic4	Emcn	Grm2	Irak1	Lrg1	Ncaph	Plxdc2	Rps21	Sumo1	Trp53
Asb2	Casp4	Cln3	Emp1	Grm3	Irak2	Lrrc25	Ncf1	Plxnb3	Rps3	Suv39h1	Trp53bp2
Ash2l	Casp6	Clstn1	eNos	Grn	Irak3	Lrrc3	Ncor1	Pmp22	Rps9	Suv39h2	Trp73
Asph	Casp7	Clu	Enpp6	Gsn	Irak4	Lsr	Ncor2	Pms2	Rrm2	Suz12	Trpa1
Atf3	Casp8	Cnn2	Entpd2	Gstm1	Irf1	Lst1	Ncr1	Pnoc	Rsad2	Syk	Trpm4
Atg14	Casp9	Cnp	Eomes	Gzma	Irf2	Lta	Nefl	Pole	Rtn4rl1	Syn2	Tspan18
Atg3	Cass4	Cntnap2	Ep300	Gzmb	Irf3	Ltb	Nfe2l2	Ppfia4	S100a10	Syp	Ttr
Atg5	Ccl2	Coa5	Epcam	H2afx	Irf4	Ltbr	Nfkb1	Ppp3ca	S100b	Tarbp2	Tubb3
Atg7	Ccl3	Col1a1	Epg5	H2-T23	Irf6	Ltc4s	Nfkb2	Ppp3cb	S1pr3	Tbc1d4	Tubb4a
Atg9a	Ccl4	Col3a1	Epsti1	Hat1	Irf7	Ly6a	Nfkbia	Ppp3r1	S1pr4	Tbr1	Txnrd1
Atm	Ccl5	Col4a1	Erbb3	Hc	Irf8	Ly6g	Nfkbie	Ppp3r2	S1pr5	Tbx21	Tyrobp
Atp6v0e	Ccl7	Col6a3	Ercc2	Hcar2	Islr2	Ly9	Ngf	Prdx1	Sall1	Tcirg1	Ugt8a
Atp6v1a	Ccng2	Cotl1	Ercc6	Hdac1	Itga6	Lyn	Ngfr	Prf1	Scd1	Tcl1	Ulk1
Atr	Ccni	Cox5b	Esam	Hdac2	Itga7	Mafb	Ninj2	Prkaca	Sell	Tet1	Ung
Axl	Ccr2	Cp	Ets2	Hdac4	Itgam	Maff	Nlg7	Prkacb	Serpina3n	Tfg	Uty
B3gnt5	Ccr5	Cpa3	Exo1	Hdac6	Itgav	Mag	Nlgn1	Prkar1a	Serpine1	Tgfa	Vamp7
Bad	Cd109	Cr2	Ezh1	Hdc	Itgax	Mal	Nlgn2	Prkar2a	Serpinf1	Tgfb1	Vav1
Bag3	Cd14	Creb1	Ezh2	Hells	Itgb5	Man2b1	Nlrp2	Prkar2b	Serping1	Tgfbr1	Vegfa
Bag4	Cd163	Crebbp	F3	Hif1a	Jag1	Map1lc3a	Nlrp3	Prkce	Sesn1	Tgm1	Vim
Bak1	Cd19	Crem	Fa2h	Hilpda	Jam2	Map2	nNos	Prkcq	Sesn2	Tgm2	Vps4a
Bard1	Cd209e	Crip1	Fabp5	Hira	Jarid2	Map2k1	Nod1	Prkdc	Setd1a	Thbd	Vps4b
Bax	Cd244	Cryba4	Fadd	Hist1h1d	Jun	Map2k4	Nostrin	Prnp	Setd1b	Tie1	Vtn
Bbc3	Cd24a	Csf1	Fancc	Hmgb1	Kat2a	Map3k1	Noxa1	Pros1	Setd2	Timeless	Was
Bcas1	Cd300lf	Csf1r	Fancd2	Hmox1	Kat2b	Map3k14	Npl	Psen2	Setd7	Timp1	Wdr5
Bcl10	Cd33	Csf2rb	Fancg	Homer1	Kcnd1	Mapk10	Npnt	Psmb8	Setdb1	Tle3	Xcl1
Bcl2	Cd36	Csf3r	Fas	Hpgds	Kcnj10	Mapk12	Nptx1	Pten	Sftpd	Tlr2	Xiap
Bcl2a1a	Cd3d	Csk	Fasl	Hprt	Kcnk13	Mapk14	Nqo1	Ptger3	Sh2d1a	Tlr4	Xrcc6
Bcl2l1	Cd3e	Cspg4	Fbln5	Hps4	Kdm1a	Mapt	Nrgn	Ptger4	Shank3	Tlr7	Zbp1
Bcl2l11	Cd3g	Cst7	Fcer1g	Hrk	Kdm1b	Marco	Nrm	Ptgs2	Siglec1	Tm4sf1	Zfp367
Bcl2l2	Cd40	Ctse	Fcgr1	Hsd11b1	Kdm2a	Mavs	Nrp2	Ptms	Siglecf	Tmc7	Aars
Bdnf	Cd44	Ctsf	Fcgr2b	Hspb1	Kdm2b	Mb21d1	Nthl1	Ptpn6	Sin3a	Tmcc3	Asb10
Becn1	Cd46	Ctss	Fcgr3	Hus1	Kdm3a	Mbd2	Nwd1	Ptprc	Sirt1	Tmem100	Ccdc127
Bid	Cd47	Ctsw	Fcrla	Icam2	Kdm3b	Mbd3	Oas1g	Ptpg1	Slamf8	Tmem119	Cnot10
Bik	Cd55b	Cx3cl1	Fcrlb	Ifi30	Kdm4a	Mbl2	Ogg1	Ptx3	Slamf9	Tmem144	Csnk2a2
Bin1	Cd59a	Cx3cr1	Fcrls	Ifih1	Kdm4b	Mcm2	Olfml3	Pycard	Slc10a6	Tmem173	Fam104a
Birc2	Cd6	Cxcl10	Fdxr	Ifitm2	Kdm4c	Mcm5	Opalin	Rab6b	Slc17a6	Tmem204	Gusb
Birc3	Cd68	Cxcl9	Fen1	Ifitm3	Kdm4d	Mcm6	Optn	Rab7	Slc17a7	Tmem206	Lars
Birc5	Cd69	Cycs	Fgd2	Ifna1	Kdm5a	Mdc1	Osgin1	Rac1	Slc1a3	Tmem37	Mto1
Blk	Cd70	Cyp27a1	Fgf13	Ifnar1	Kdm5b	Mdm2	Osmr	Rac2	Slc2a1	Tmem64	Supt7l
Blm	Cd72	Cyp7b1	Fgl2	Ifnar2	Kdm5c	Mef2c	P2rx7	Rad1	Slc2a5	Tmem88b	Tada2b
Blnk	Cd74	Cytip	Fkbp5	Ifng	Kdm5d	Mertk	P2ry12	Rad17	Slc44a1	Tnf	Tbp
Bmi1	Cd83	Dab2	Flt1	Igf1	Kdm6a	Mfge8	Pacsin1	Rad50	Slc6a1	Tnfrsf10b	Xpnpep1
Bnip3	Cd84	Dapk1	Fn1	Igf1r	Kif2c	Mgmt	Padi2	Rad51	Slco2b1	Tnfrsf11b	
Bnip3l	Cd86	Dcx	Fos	Igf2r	Klr3dl1	Mmp12	Pak1	Rad51b	Slfn8	Tnfrsf12a	

Analysis of data from a previous study [63] of gene expression in WT mice at an acute time point is included in this paper for historical perspective and to visualize our full-time course in one location (Fig. 7). The experimental methods in the previous study have been published [63], and were the same as those used in the current study. Note that since the last study, we have expanded the panel of genes from 791 genes to 826 genes.

3. Results

3.1. Overall gene expression

Our first metric for evaluation was to examine the expression of genes in the neuroinflammatory pathway over the 4WK, 8WK, and 16WK post-surgery time points compared to the pre-surgical naïve sham mice (Non-Surgical Control or NSCTR). The neuroinflammatory panel contained 813 experimental genes of interest and 13 housekeeping genes. First, 242 genes were removed from analysis based on the exclusion criteria leaving 571 genes to be discussed. The Venn diagram shows the number of genes differentially expressed at each time point (Fig. 1). Only two genes, *Tnfrsf25* and *Arc*, showed downregulation at any point examined (Table 2). Gene counts in the overlapping regions are different genes than those reported in the non-overlapping regions, indicating that the same gene was differentially expressed at each time point that overlaps in the diagram.

Overall, we identified 28 of the 813 neuroinflammatory genes examined to be differentially expressed at any of the post-surgical time points (4WK, 8WK, and 16WK), with 19 genes showing stable upregulation at all three time points (Fig. 1, Table 2). Specifically, 25 genes were differentially expressed at 4WK, 20 were differentially expressed at 8WK, and 24 were differentially expressed at 16WK.

At 4WK post-surgery, 23 genes were identified to be upregulated, and two were determined to be downregulated compared to NSCTR (Fig. 1, Table 2). At 8WK post-surgery, 19 of the 23 differentially expressed genes upregulated at 4WK remain upregulated, and no additional genes were newly upregulated (Fig. 1, Table 2). Additionally, only one of the two genes downregulated at 4WK remained so at 8WK (*Tnfrsf25*, Table 2). In total, 20 of the 25 differentially expressed genes at 4WK remain differentially expressed at 8WK. The five genes differentially expressed at 4WK but not at 8WK include *Arc, C3ar1, Fcer1g, Lnc2, and Ptx3.*

At 16WK post-surgery, the gene downregulated at both 4WK and 8WK post-surgery, *Tnfrsf25*, was no longer downregulated. Nineteen genes upregulated at 4WK and 8WK remained so at 16WK; thus, these 19 genes were upregulated at all three time points examined (Fig. 1, Table 2). Additionally, three genes are newly upregulated at 16WK (*Anxa1, Blnk*, and *H2-T23*), and two genes that were upregulated at 4WK but not 8WK surpassed the upregulation threshold again ($P_{adj} < 0.05$ and Log2FoldChange > 1 or < -1) at 16WK (*Fcer1g* and *Lcn2*).

In total, compared to NSCTR, 25 genes were differentially expressed at 4WKs post-surgery with 23 upregulations, 20 genes were differentially expressed at 8WKs post-surgery with 19 upregulations, and 24 genes were upregulated at 16 WKs post-surgery.

While the Venn diagram summarizes the trends for differential gene expression, we also utilized volcano plots to illustrate the Log2FoldChange of each gene at each time point (4WK, 8WK, 16WK) compared to NSCTR (Fig. 2). Volcano plots allow for visualization of the statistical significance and the magnitude of change in expression levels. Fig. 2 visualizes and labels each gene showing differential expression above statistical significance ($P_{adj} > 0.05$) and Log2FoldChange > 1 or < -1 (linear fold change > 2 or < -2).

Table 2
Gene expression at the microelectrode-tissue interface. Differentially expressed genes at 4WK, 8WK, and 16WK post-surgery are listed. Genes with differential expression of $P_{adj} < 0.05$ and Log2FoldChange > 2 or < -2 are in green; genes with differential expression of $P_{adj} < 0.05$ and Log2FoldChange between 1 – 2 and -1 to -2 are in blue. The molecular pathway these genes fall under is listed in Table 3.

4WK				8WK				16WK			
Gene	Log2 Fold Change	std error (log2)	Padj	Gene	Log2 Fold Change	std error (log2)	Padj	Gene	Log2 Fold Change	std error (log2)	Padj
								Anxa1	1.42	0.417	0.0199
Arc	-1.14	0.305	0.0106								
Bcl2a1a	1.64	0.272	2.78E-05	*Bcl2a1a*	1.25	0.275	0.0018	*Bcl2a1a*	1.56	0.273	7.39E-05
								Blnk	1.13	0.224	0.0004
C3	2.64	0.554	0.0008	*C3*	2.48	0.556	0.0019	*C3*	3.53	0.546	8.77E-06
C3ar1	1.22	0.302	0.0050								
C4a	3.01	0.335	1.84E-08	*C4a*	3.08	0.335	1.54E-08	*C4a*	3.48	0.334	1.15E-09
Cd36	2.66	0.641	0.0042	*Cd36*	2.86	0.64	0.0019	*Cd36*	2.76	0.64	0.0027
Cd68	1.45	0.237	2.65E-05	*Cd68*	1.20	0.238	0.0005	*Cd68*	1.31	0.237	0.0001
Cd74	1.93	0.478	0.0050	*Cd74*	2.00	0.477	0.0037	*Cd74*	1.78	0.478	0.0106
Cd84	1.47	0.247	3.41E-05	*Cd84*	1.38	0.248	0.0001	*Cd84*	1.49	0.247	3.02E-05
Clec7a	3.20	0.47	3.74E-06	*Clec7a*	2.81	0.474	5.50E-05	*Clec7a*	3.15	0.47	4.81E-06
Ctss	1.34	0.177	6.35E-07	*Ctss*	1.20	0.177	6.96E-06	*Ctss*	1.26	0.177	2.32E-06
Fcer1g	1.20	0.218	0.0001					*Fcer1g*	1.03	0.219	0.0010
Fcgr2b	1.66	0.253	6.89E-06	*Fcgr2b*	1.52	0.253	5.34E-05	*Fcgr2b*	1.71	0.253	4.25E-06
Gfap	2.45	0.355	3.56E-06	*Gfap*	2.12	0.355	5.34E-05	*Gfap*	2.41	0.355	4.25E-06
								H2-T23	1.22	0.217	9.46E-05
Lcn2	1.89	0.494	0.0084					*Lcn2*	1.84	0.494	0.0106
Lilrb4a	2.85	0.472	2.78E-05	*Lilrb4a*	2.53	0.474	0.0003	*Lilrb4a*	2.50	0.474	0.0002
Mpeg1	1.56	0.211	9.94E-07	*Mpeg1*	1.30	0.212	4.24E-05	*Mpeg1*	1.50	0.211	2.32E-06
Mmp12	5.41	0.561	4.75E-09	*Mmp12*	5.39	0.561	1.03E-08	*Mmp12*	5.66	0.561	1.41E-09
Psmb8	1.04	0.265	0.0070	*Psmb8*	1.27	0.263	0.0009	*Psmb8*	1.16	0.264	0.0022
Ptx3	1.87	0.431	0.0024								
Serpina3n	2.53	0.251	2.84E-09	*Serpina3n*	2.20	0.253	4.23E-08	*Serpina3n*	2.41	0.251	3.43E-09
Spp1	3.46	0.398	3.32E-08	*Spp1*	3.31	0.398	9.93E-08	*Spp1*	3.78	0.398	3.43E-09
Tnfrsf25	-1.36	0.276	0.0006	*Tnfrsf25*	-1.22	0.275	0.0019				
Tyrobp	1.22	0.208	3.68E-05	*Tyrobp*	1.07	0.208	0.0004	*Tyrobp*	1.14	0.208	0.0001
Vim	1.71	0.25	3.74E-06	*Vim*	1.44	0.251	8.85E-05	*Vim*	1.73	0.25	3.36E-06

Overall gene expression is stable between 4WK to 16WK post-surgery: expression change skews towards upregulation, with more genes showing upregulation than downregulation. Most genes show differential expression below statistical significance ($P_{adj} > 0.05$), and of those genes showing upregulation above statistical significance, most show a Log2FoldChange > 1 or < -1 (which corresponds to linear fold change > 2 or < -2).

Genes with differential expression at 4WK, 8WK, and 16WK post-surgery compared to NSCTR above the threshold of Log2FoldChange > 1 or < -1 are listed in Table 2. Additionally, genes with differential expression above a higher threshold of Log2FoldChange > 2 or < -2 are labeled in green, which are: *C3, C4a, Cd36, Clec7a, Gfap Lilb4a, Mmp12, Serpina3n*, and *Spp1.* These nine genes, which show the highest upregulation at 4–16WK post-surgery, show upregulation above the threshold of Log2FoldChange > 2 or < -2 at all post-surgical time points in this study. *Mmp12* is the highest expressed gene at all time points examined in this study, with Log2FoldChange between 5.39 – 5.99.

The pathways associated with the differentially expressed genes in Table 2 are listed in Table 3. These differentially expressed genes identified in this study are enriched for proteins involved in neutrophil degranulation, complement system, cell surface receptors (pattern recognition receptors and others), extracellular matrix, and adaptive immune system. Some genes fall into several categories.

4. Specific gene differential expressions

4.1. Complement system

The complement system is part of the innate immune system and consists of circulating proteins, cell surface regulators, and effectors. The complement system is activated by invading pathogens and tissue damage via classical, lectin-binding, and alternative pathways, converging at the amplification step of C3 [76]. The protein C3 is a critical molecule in the amplification step of the complement activation cascade, and the protein C4a is a subunit of C4 and a by-product of C4 activation. C4 is also involved in the amplification step of the complement activation cascade.

Fig. 3 a (and Table 2) compares the gene complement 3 (*C3*) between each post-surgical time point evaluated in the study. At 4WK and 8WK post-surgery, *C3* expression displayed 2.64X and 2.48X Log2FoldChange compared to NSCTR. At 16WK post-surgery, *C3* expression increased to 3.53X Log2FoldChange compared to NSCTR. However, a comparison between 8WK or 16WK post-surgery to 4WK post-surgery and between 8WK and 16WK post-surgery showed no statistically significant differential expression between each pair. The gene *complement 4 subunit a* (*C4a*) demonstrated a similar trend (Fig. 3b, Table 2), showing 3.01X and 3.08X Log2FoldChange compared to NSCTR at 4WK and 8WK post-surgery, and slightly increased to 3.48X Log2FoldChange at 16WK

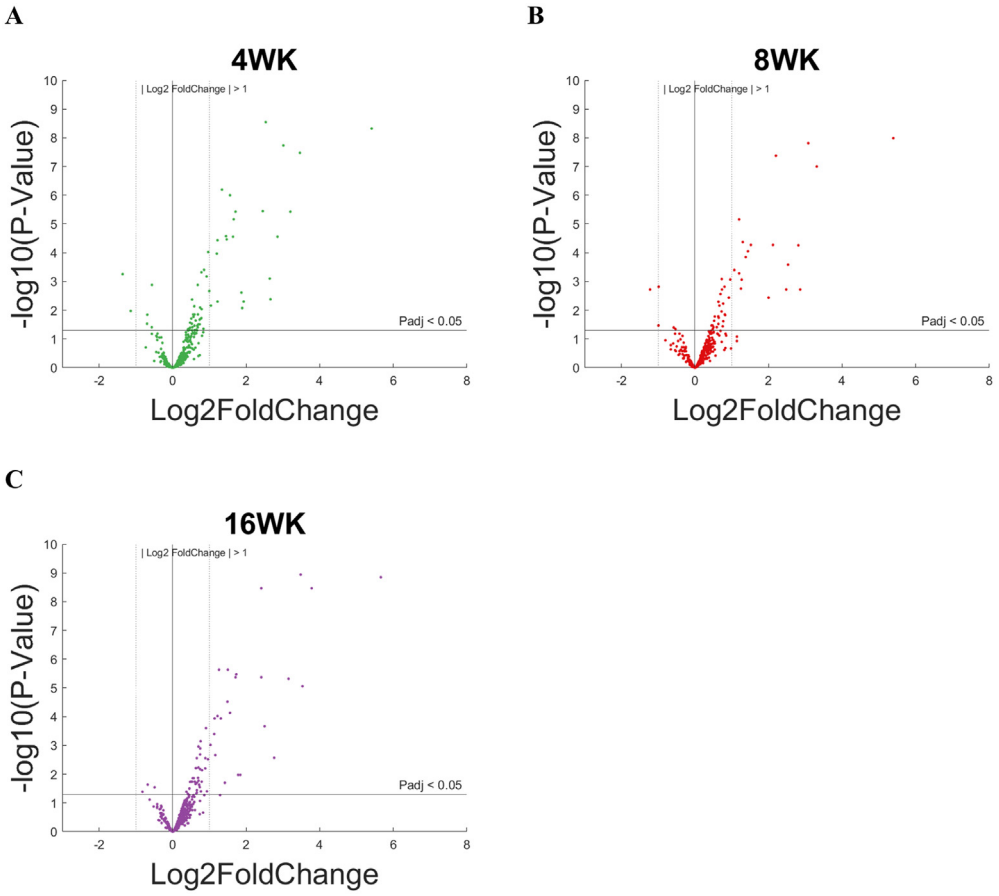

Fig. 2. Volcano plots of genes with differential expression at (a) 4WK, (b) 8WK, and (c) 16WK compared to NSCTR. Genes with differential expression of Log2FoldChange > 1 or < -1 and P_{adj} < 0.05 are labeled.

post-surgery. Genes encoding for both the receptor for C3 subunit a (*C3ar1*) and pentraxin-3 (*Ptx3*) showed a significant (1.22X and 1.87X, respectively) Log2FoldChange compared to NSCTR at 4WK post-surgery (Fig. 3c-d, Table 2). Note that for *C3ar1* expression at 16WK, Log2FoldChange < 1 (0.848) compared to NSCTR, below the threshold of Log2FoldChange > 1 or < -1; therefore, *C3ar1* did not meet the criteria for differential expression at 16WK post-surgery. Like the trend displayed for *C3*, for *C4a, C3ar1*, and *Ptx3*, pairwise comparison between 4WK, 8WK, and 16WK post-surgery showed no statistically significant differential expression between any of these pairs – indicating no changes in expression over 4WK to 16WK post-surgery.

4.2. Extracellular matrix

The extracellular matrix forms a scaffold around the cells in the brain and maintains tissue integrity and communication between cells [77]. During injury and inflammation of brain tissue, such as following the implantation of microelectrodes, the extracellular matrix is actively remodeled as part of the wound healing process [78,79].

Fig. 4 and Table 2 highlights the genes examined in our set that encode proteins associated with the extracellular matrix and displayed significance indicated by P_{adj} < 0.05. In Fig. 4a (Table 2). Our results demonstrate that the expression of genes encoding for Matrix Metallopeptidase 12 (*Mmp12*) show a 5.41X, 5.39X, and 5.66X Log2FoldChange compared to NSCTR at 4WK, 8WK, and 16WK post-surgery, respectively. The expression of *Mmp12* was detected as stable throughout the study; pairwise comparison between 4WK, 8WK, and 16WK showed no significant difference in expression levels between any of the three examined time points. Genes encoding for Secreted Phosphoprotein 1 (*Spp1,* Fig. 4b and Table 2) also showed a stable upregulation over the course of this study: 3.46X, 3.31X, and 3.78X Log2FoldChange at 4WK, 8WK, and 16WK post-surgery, respectively. Genes encoding for Cathepsin S (*Ctss,* Fig. 4c and Table 2) show a stable upregulation of 1.34X, 1.20X, 1.26X Log2FoldChange compared to NSCTR at 4WK, 8WK, and 16WK post-surgery, respectively. As with *Mmp12* and *Spp1, Ctss* expression was statistically unchanged from 4WK to 16WK post-surgery. All three genes associated with the extracellular matrix that demonstrated a significant change in expression level (P_{adj} < 0.05 for comparisons between the time point and NSCTR) displayed consistent expression levels, regardless of the duration post-implantation.

4.3. Cellular receptors

Cellular responses to the environment, or environmental changes, are primarily facilitated through receptor-ligand interactions. In this section, we group several classes of cellular receptors involved in the neuroinflammatory response. Here, cell receptors associated with the pattern recognition receptor (PRR) family (*Cd36, Clec7a*), receptors for immunoglobulins (*Fcer1g, Fcgr2b*), as well as leukocyte-associated immunoglobulin-like receptors (*Lilrb4a*) are discussed due to their significant changes following microelectrode implantation (Fig. 5 and Table 2).

Fig. 5a and Table 2 demonstrates that expression of Cluster of Differentiation 36 (*Cd36*) showed a steady Log2FoldChange of 2.66X, 2.86X, 2.76X compared to NSCTR at 4WK, 8WK, and 16WK post-surgery. A pairwise comparison between 4WK, 8WK, and

Table 3
The molecular pathways of differentially expressed genes at 4WK, 8WK, or 16WK post-surgery (threshold at Log2FoldChange > 1 or < -1, $P_{adj} < 0.05$). The Log2FoldChange, Std Error in log_2 and P_{adj} of these genes are listed in Table 2.

Genes	Full name of Genes	Neutrophil Degranulation	Complement System	PRR/ IgR	Extracellular Matrix	Adaptive Immune System	Others
Anxa1	Annexin A1						Intracellular Signaling
Arc	Activity Regulated Cytoskeleton Associated Protein						Intracellular Signaling
Bcl2a1a	BCL2 Related Protein A1						apoptosis
Blnk	B-cell linker					yes	Intracellular Signaling
C3	Complement C3	yes	yes			yes	Intracellular Signaling, Metabolism
C3ar1	Complement C3a Receptor 1	yes	yes				Intracellular Signaling
C4a	Complement C4A		yes				
Cd36	Cluster of Differentiation 36	yes		yes		yes	metabolism, Vesicle-mediated transport Cell Adhesion
Cd68	Cluster of Differentiation 68						
Cd74	Cluster of Differentiation 74					yes	
Cd84	Cluster of Differentiation 84						
Clec7a	C-Type Lectin Domain Family 7 Member A			yes			
Ctss	Cathepsin S	yes		yes	yes	yes	
Fcer1g	Fc Epsilon Receptor Ig	yes		yes			
Fcgr2b	Fc Gamma Receptor IIb	yes		yes		yes	
Gfap	Glial Fibrillary Acidic Protein						Cytoskeleton
H2-T23	H2-T23	yes				yes	
Lcn2	Lipocalin 2	yes					Transport of small molecules
Lilrb4a	Leukocyte Immunoglobulin Like Receptor B4	yes					
Mmp12	Matrix Metalloprotease 12				yes		
Mpeg1	Macrophage Expressed 1						Anti-microbial
Psmb8	Proteasome 20S Subunit Beta 8					yes	Cytokine, cell cycle, transcription
Ptx3	Pentraxin	yes	yes				
Serpina3n	Serpin Family A Member 3						protease
Spp1	Secreted Phosphoprotein 1				yes		Intracellular Signaling, Metabolism
Tnfrsf25	TNF Receptor Superfamily Member25						Cytokine Receptor, Intracellular Signaling
Tyrobp	Transmembrane Immune Signaling Adaptor TYROBP	yes					Developmental Biology
Vim	vimentin						cytoskeleton

16WK showed that *Cd36* expression levels were not significantly different.

Fig. 5b and Table 2 demonstrated that genes encoding for C-Type Lectin Domain Family 7 Member A (*Clec7a*) showed an upregulation of 3.20X, 2.81X, 3.15X Log2FoldChange at 4WK, 8WK, and 16WK post-surgery, respectively. Expression levels were highest at 4WK and 16WK post-surgery. However, pairwise comparison showed that expression levels at 8WK post-surgery were not significantly different from those at 4WK or 16WK. Genes encoding for Leukocyte Immunoglobulin Like Receptor B4 (*Lilrb4a*) showed an upregulation in Log2FoldChange of 2.85X, 2.53X, and 2.50X at 4WK, 8WK, and 16WK post-surgery, respectively (Fig. 5c and Table 2). Pairwise comparison showed that expression levels at 4WK post-surgery were not significantly different from those at 8WK or 16WK.

Genes encoding for IgE receptor Fc E Receptor 1g (*Fcer1g*, Fig. 5d and Table 2) and IgG receptor Fc G Receptor 2b (*Fcgr2b*, Fig. 5e and Table 2) showed a small yet consistent upregulation at 4WK to 16WK post-surgery. *Fcer1g* showed Log2FoldChange of 1.2X and 1.03X at 4WK and 16WK post-surgery. Note that at 8WK post-surgery, the Log2FoldChange < 1 (0.921) compared to NSCTR; therefore, *Fcer1g* did not meet our criteria as differentially expressed at 8WK post-surgery. *Fcgr2b* showed 1.66X, 1.52X, and 1.71X Log2FoldChange compared to NSCTR at 4WK, 8WK, and 16WK post-surgery, respectively. While the expression level of *Fcgr2b* decreased slightly from 4WK to 8WK, only to increase again at 16WK, each time point showed significantly higher *Fcgr2b* expression than NSCTR, and pairwise comparison indicated that the expression at each time point was not statistically different from each other.

4.4. Other highly differentially expressed genes

Genes encoding for *Gfap* displayed a consistently elevated expression level of 2.45X, 2.12X, and 2.41X Log2FoldChange at 4WK, 8WK, and 16WK post-surgery. Further, there were no significant differences in the expression levels between each time point pair (Fig. 6a, Table 2). Genes encoding for Serine peptidase inhibitor clade A member 3n (*Serpina3n*) showed a Log2FoldChange of 2.53X, 2.20X, and 2.41X at 4WK, 8WK, and 16WK post-surgery compared to NSCTR. No statistically significant differences were detected between any time point pairs, indicating that *Serpina3n* gene expression was stably upregulated throughout this study (Fig. 6b, Table 2).

4.5. Considering gene expression acute time points

To better chronicle the differential expression of genes over time, data from a previous study that used the same methodology used here but for acute time points of 6H, 24H, 72H, and 2WK post-surgery [63] were included in the current chronic data set. The present study used an expanded panel of 826 genes compared to the 791 in the original study. The pre-surgical, naïve sham

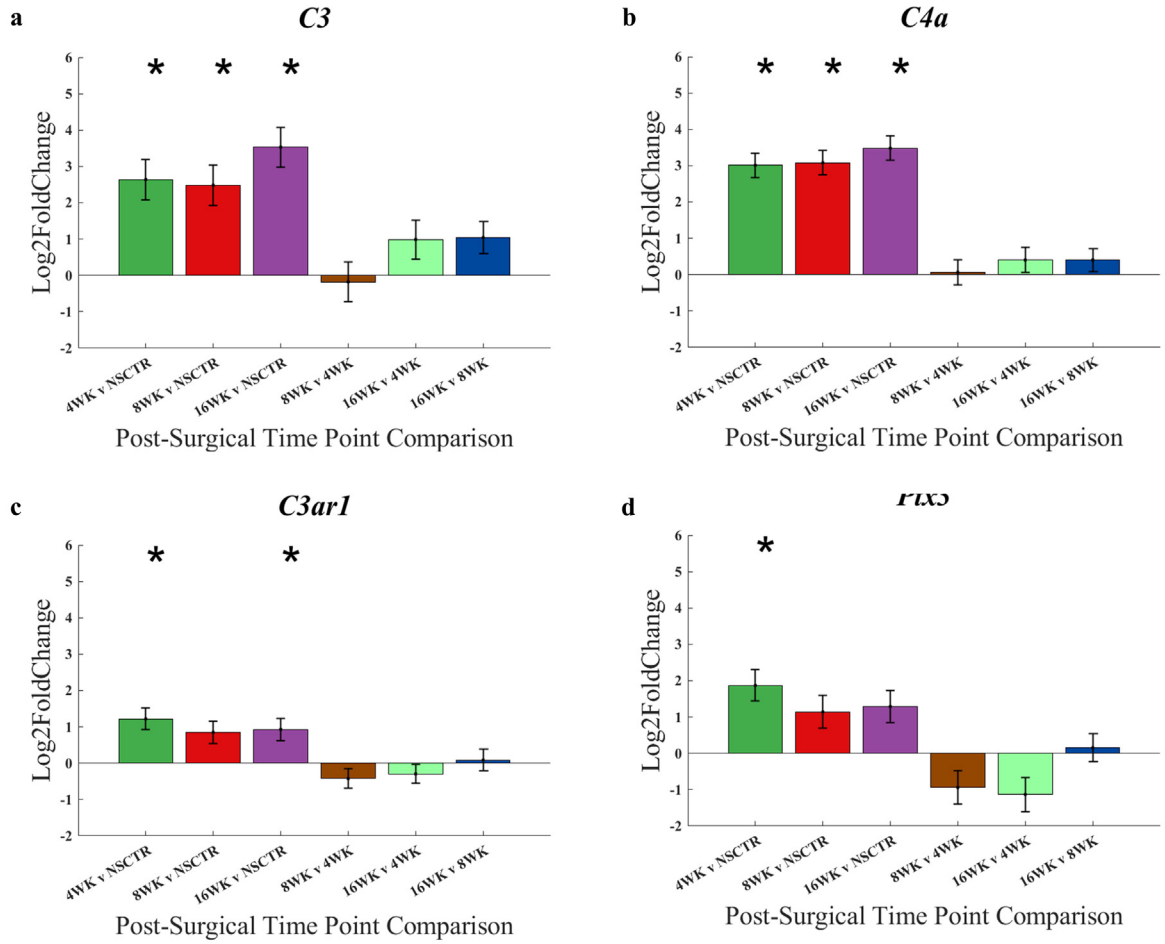

Fig. 3. Bar graphs presenting the differential gene expression of (a) *C3*, (b) *C4a*, (c) *C3ar1*, and (d) *Ptx3* at 4WK vs. NSCTR (green), 8WK (red) vs. NSCTR, and 16WK vs. NSCTR (purple), 4WK vs. 8WK (brown), 4WK vs. 16WK (lime green), and 8WK vs. 16 WK (navy blue). The height of each bar illustrates the Log2FoldChange of the comparison. The error bar indicates the standard error of the mean between gene expressions at each time point. Asterisk (*) denotes $P_{adj} < 0.05$.

control used in the previous study (NSCTR) discussed in this section is a different set of animals from those used in the current study.

Of the 791 genes investigated in the previous study, 13 are housekeeping genes used for normalization. Of the remaining 778 genes, 189 were removed from analysis based on the exclusion criteria, leaving 589 genes to be discussed. Of the 589 genes, 61 showed no differential expression at any time point in the study (not represented below). In total, 536 genes showed differential expression at 6H, 24H, 72H, or 2WK post-surgery. The Venn diagram (Fig. 7) indicates the number of genes differentially expressed at each time point in the previous study.

Overall, there are 65 genes showing differentially expressed throughout 6H to 2WK post-surgery. At 6H post-surgery, a total of 153 genes showed differential expression. One gene showed differential expression at only 6H post-surgery. At 24H post-surgery, 501 genes showed differential expression, including 151 genes exhibiting differential expression at 6H post-surgery and 350 newly differentially expressed genes. Eighty-nine genes showed differential expression at only 24H post-surgery. At 72H post-surgery, 181 genes showed differential expression, including 175 that showed differential expression at 24H post-surgery and six newly differentially expressed genes. One gene showed differential expression at only 72H post-surgery. No genes showed differential expression at 6H and 72H but not 24H post-surgery. At 2WK, 358 genes showed differential expression, with 139 maintaining differential expression from 72H. One hundred sixty-five genes showed differential expression at only 24H and 2WK, 34 showed differential expression at 6H, 24H, and 2WK, and one gene showed differential expression at 6H and 2WK. Nineteen genes showed differential expression at 2WK only.

5. Discussion

Overall, by chronic time points (4WK to 16WK), fewer genes show differential expression compared to acute time points (6H to 2WK), and the gene expression becomes more stable. Most of the 28 genes exhibiting differential expression at 4WK to 16WK are in the complement, extracurricular, or cell receptor pathways. Nineteen of these genes show overexpression at 4WK, 8WK, and 16WK post-surgery and exhibit a similar expression level at these time points. Therefore, at 4WK to 16WK post-surgery, the ongoing neuroinflammation and neurodegeneration are driven stably by a specific set of complement, extracurricular, or cell receptor pathways.

5.1. Complement system

In previous studies, we have found that many members of the complement system displayed high upregulation at acute time points (6H to 2WK) post-surgery, with C3 showing increasing upregulation over the course of 6H to 2WK post-surgery [63,68]. Many labs have identified C3 as an essential player in neuroinflammatory response to intracortical microelectrode implantation and suggested that inhibition of C3 could result in a potential ther-

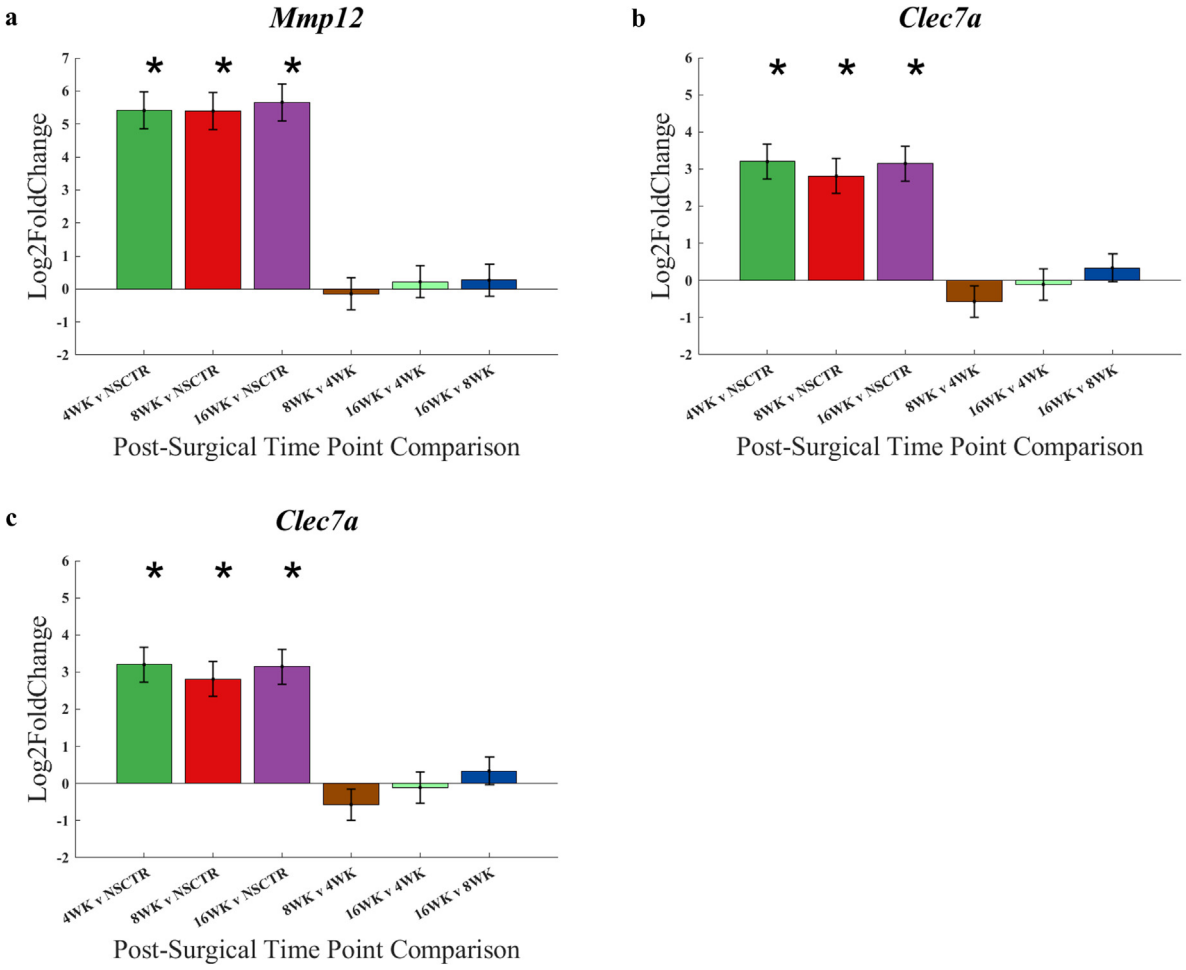

Fig. 4. Bar graph of differential gene expression of (a) *Mmp12*, (b) *Spp1,* and (c) *Ctss* at 4WK vs. NSCTR (green), 8WK vs. NSCTR (red), and 16WK vs. NSCTR (purple), 4WK vs. 8WK (brown), 4WK vs. 16WK (lime green), and 8WK vs 16 WK (navy blue). The height of each bar shows the Log2FoldChange of the comparison. The error bar indicates the standard error of the mean between gene expressions at each time point compared. Asterisk (*) denotes $P_{adj} < 0.05$ for the time point and NSCTR comparisons.

apeutic target [63–65,68]. *C4a* codes for a subunit of C4 and a marker of C4 activation; C4 activation is upstream of C3 activation [80]. *C3ar1* codes for the cellular receptor of C3a, a subunit of C3 and a marker of C3 activation [80]. Pentraxin-3 (*Ptx3*) is an acute-phase protein that regulates the immune system, including the complement system [81,82].

In addition to its role in innate immunity against various pathogens, the complement system is also responsible for foreign body response against biomaterials [83–85]. The complement cascade is activated by the adsorbed IgG or C3 directly on the biomaterial surface, which occurs immediately after biomaterial implantation. The adsorption leads to the activation of cellular responders and the production of pro-inflammatory cytokines and chemokines, activating an immune response against microelectrodes [86–88]. To date, we are unaware of any report directly linking the complement system's role and the failure of intracortical microelectrodes. However, the upregulation of complement factors suggests its role in tissue response against microelectrodes. The sustained upregulation of members of the complement system indicates that this process still occurs at chronic time points and may contribute to tissue response against microelectrodes at both acute and chronic time points.

5.2. Extracellular matrix

Matrix Metallopeptidases 12 (*Mmp12)* is a Matrix Metalloproteinase (MMPs) family member. MMPs are zinc-containing endopeptidases that participate in the remodeling of extracellular matrix by breaking down extracellular matrix into its components [89]. In a previous study by Rennaker *et al.*, rats administered with Minocycline showed improved neural recording performances [46]. Minocycline is an antibiotic and a broad-spectrum immune modulator. Minocycline may reduce the neuroinflammatory response and limit post-surgical microbial infection, increasing microelectrode integration in the study. In addition, minocycline is a non-specific MMP inhibitor and may have also influenced extracellular matrix remodeling, providing an alternative pathway to microelectrode recording performance [90,91]. It is important to note that the mechanisms of action for Minocycline were not explored in detail in the initial Rennaker *et al.* manuscript or any follow-up studies.

Secreted Phosphoprotein 1 (*Spp1*) is a part of the extracellular matrix of the central nervous system (CNS) and of the bone matrix, as well as a cytokine that regulates the immune response of the CNS [92]. In the CNS, macrophages express *SPP1, which* may activate microglia and contribute to neurodegeneration [92–94]. Cathepsin S (*Ctss*) is associated with extracellular matrix remodeling in the body, and its overexpression is associated with pulmonary fibrosis or aberrant extracellular matrix expression in the lungs [95]. Although the role of *Ctss* in extracellular matrix remodeling in the brain has not been extensively studied, *Ctss* is expressed by microglia in the central nervous system [96] and thus may play a role in glial scar formation around implanted intracortical microelectrodes.

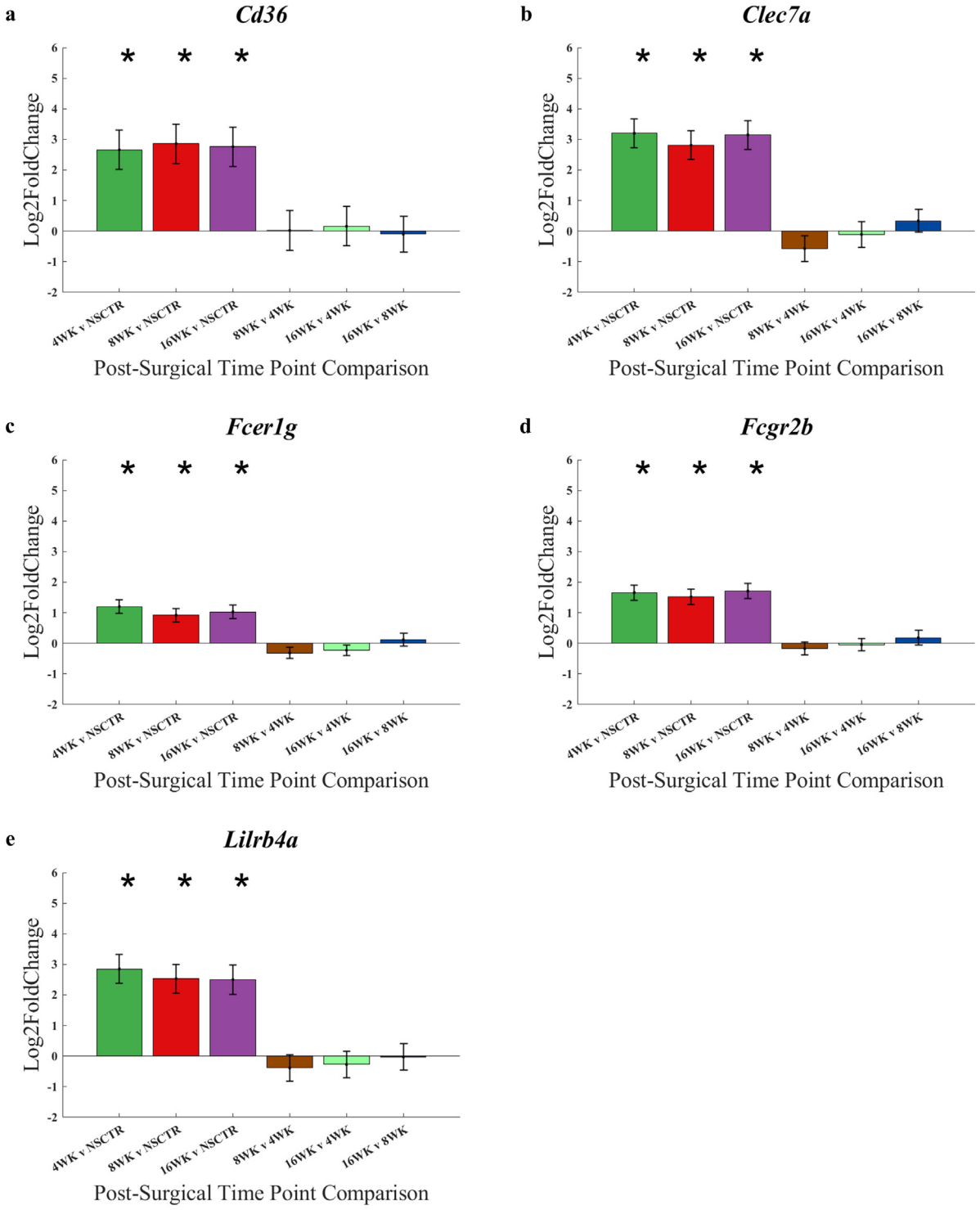

Fig. 5. Bar graph of differential gene expression of (a) *Cd36*, (b) *Clec7A*, (c) *Lilrb4a*, (d) *Fcer1g*, and (e) *Fcgr2b* at 4WK vs. NSCTR (green), 8WK vs. NSCTR (red), 16WK vs. NSCTR (purple), 4WK vs. 8WK (brown), 4WK vs. 16WK (lime green), and 8WK vs. 16 WK (navy blue). The height of each bar shows the Log2FoldChange of comparison. The error bar indicates the standard error of the mean between gene expressions at each time point compared. Asterisk (*) denotes $P_{adj} < 0.05$.

The extracellular matrix (ECM) in the central nervous system is unique compared to the rest of the body, consisting of minimal collagen and fibronectin, which are a significant component of the extracellular matrix for the rest of the body, and mainly comprised of proteoglycans, glycoproteins, linker proteins, and matricellular proteins [97,98]. Since ECM support allows for the communication between cells in the CNS, remodeling of the ECM may affect neuronal, microglial, astrocytic, and oligodendrocytic activity in the tissue microelectrode interface, contributing to the chronic failure of microelectrode recording. Further, being that all three genes associated with the ECM that were detected to significantly change expression levels compared to NSCTR were consistently expressed at 4WK, 8WK, and 16WK post-surgery, our interpretation of the results is that the post-implantation ECM expression/composition is matured by 4WKs and remains stable throughout the remaining duration of microelectrode implantation. Therefore, changes in

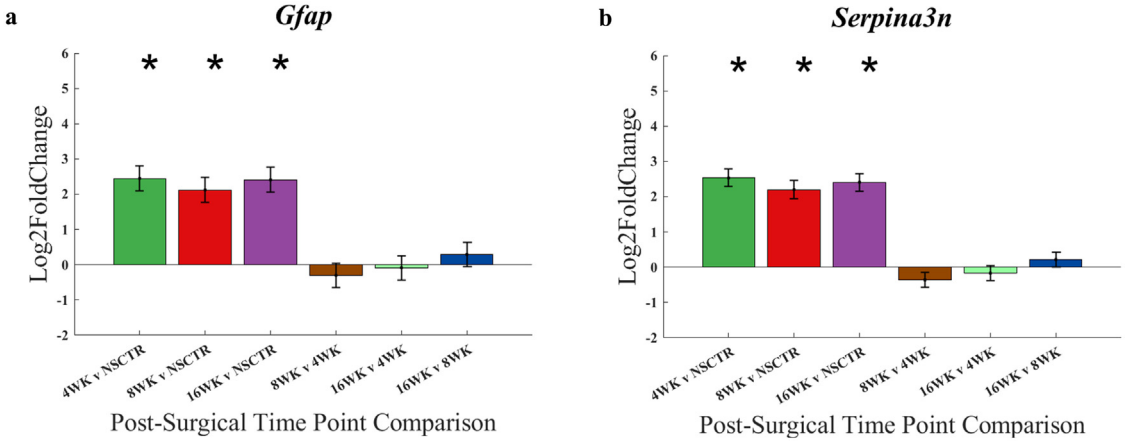

Fig. 6. Bar graph of differential gene expression of (a) *Gfap* and (b) Serpina3n at 4WK vs. NSCTR (green), 8WK vs. NSCTR (red), and 16WK vs. NSCTR (purple), 4WK vs. 8WK (brown), 4WK vs 16WK (lime green), and 8WK vs 16 WK (navy blue). The height of each bar shows the Log2FoldChange of comparison. The error bar indicates the standard error of the mean between gene expressions at each time point compared. Asterisk (*) denotes $P_{adj} < 0.05$.

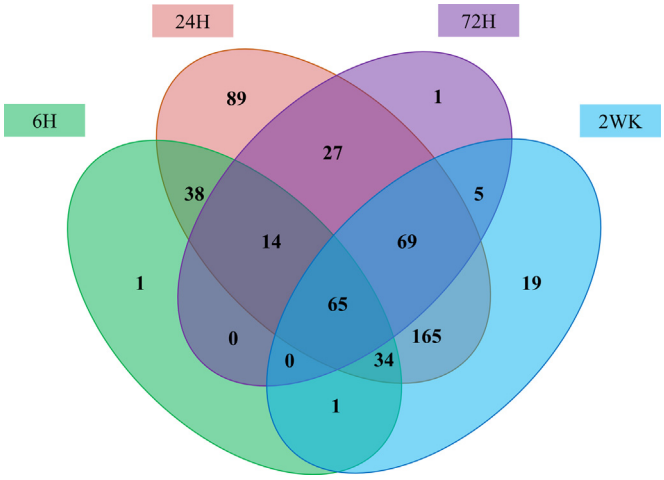

Fig. 7. Gene expression at the microelectrode-tissue interface in acute time points. a) Venn Diagram indicating the number of genes differentially expressed for each time point examined, compared to the NSCTR mice at acute time points, based on data from a previously published study [63]. Overlapping regions of the Venn diagrams were used to show an overlap of differentially expressed genes at 4WK, 8WK, and 16WK post-surgery compared to naïve sham control mice, $P_{adj} < 0.05$ and Log2FoldChange > 1 or < -1.

recording performance between 4WK to 16WK post-surgery are likely not a result of changes in the extracellular matrix composition alone. However, immunohistology images of ECM proteins adjacent to microelectrode arrays have shown changes in the distribution of ECM components with time [65,99–103].

5.3. Cellular receptors

Cluster of Differentiation 36 (Cd36) is a glycoprotein expressed on the surface of platelets and macrophages. Cd36 is a scavenger receptor that recognizes thrombospondin, collagen, phospholipids, as well as oxidized LDL; and is a coreceptor for TLR4:TLR6 complex [104–106], leading to activation of macrophages via intracellular signaling pathway. Further, Cd36 also functions as an adhesion molecule [106,107]. C-Type Lectin Domain Family 7 Member A (Clec7a) is a glycoprotein on the surface of macrophages and B-lymphocytes with a C-lectin-like extracellular domain. Clec7a is a pattern recognition receptor that detects fungi and can lead to the activation of immune cells, as well as a co-stimulator of T-cells promoting T-cell activation [108–110]. Leukocyte Immunoglobulin-like receptor Superfamily B member 4 (Lilr4a) is a glycoprotein expressed on macrophages and recognized MHCI expressed on antigen-presenting cells (APCs) [111]. Lilr4a downregulates the activation of macrophages and downregulates immune activity [111,112]. *Fcer1g* encodes for a receptor for the Fc segment of IgE, while *Fcgr2b* encodes for a receptor for the Fc segment of IgG. *Fcer1g* and *Fcgr2b* are expressed in astrocytes and microglia to facilitate the inflammatory response to immunoglobulins [113]. While the specific activities of each of these five genes are varied, the upregulation of them together likely reflects a well-coordinated and highly specified cell-mediated inflammatory response triggering further immune cell activation to chronic microelectrode implants. Receptor-ligand interactions have been a target of the biomaterials host response field for decades [114] and, more specifically, approached by those seeking to inhibit microelectrode-induced tissue responses [115,116]. The receptors indicated here could represent future targets to mitigate cellular responses to events following microelectrode implantation to improve chronic recording performance.

5.4. Other highly differentially expressed genes

Increased expression of glial fibrillary acidic protein (GFAP) is a marker for reactive astrocytosis or glial scar formation and a well-established marker for neuroinflammatory tissue response in the context of microelectrode implantation [31,32,71,117] – hence it was one of the custom-added genes to our custom assay set. *Gfap* gene expression is therefore congruent with our understanding of tissue response to intracortical microelectrodes that GFAP protein is stably upregulated at 4WK to 16WK time points post-implantation. *Serpina3n* encodes for the protein serine peptidase inhibitor clade A member 3n, and it is orthologous to a1-antichymotrypsin in humans. *Serpina3n* inhibits the proteolytic activity of Cathepsin G, leukocyte elastase, granzyme B, and matrix metallopeptidase 9 [118]. *Serpina3n* is often expressed in neurons and astrocytes after injury [119] and is overexpressed in mouse models of Alzheimer's and prion disease [120]. There are conflicting reports on the role of *Serpina3n* in neuroinflammation. Multiple studies have found *Serpina3n* to be neuroprotective: higher *Serpina3n* expression is associated with attenuating neuropathic pain, reducing the severity of Multiple Sclerosis, and reducing tissue damage in ischemic stroke [121]. Thus, higher expression of *Serpina3n* at chronic time points reported here may represent the upregulation of neuroprotective molecules after the initial neuroinflammatory response of the acute phase has begun to subside.

However, in one study of mice treated with neurotoxin, the neuroprotective effect of melatonin was lost when associated with serpina3n overexpression [122]. Therefore, a controlled study intentionally overexpressing or inhibiting *Serpina3n* expression in an intracortical microelectrode implant model may resolve conflicting results.

5.5. Considering gene expression acute time points

While differential gene expression at chronic time points following microelectrode implantation is relatively stable, the differential gene expression at acute time points is more dynamic. The acute response has more upregulated genes, based on a related study using the same methods and also analyzed with nCounter technologies [63]. Of the 791 genes we investigated in the previous study (Note: in our current study, we used 826 genes as we expanded our panel) at 6H, 24H, 72H, and 2WK post-surgery, 65 genes were upregulated at all time points. There are 1, 89, 1, and 19 genes that are differentially expressed at only one of the time points, 6H, 24H, 72H, and 2WK post-surgery, respectively.

6. Conclusions

In this study, we investigated the expression of 826 genes in the neuroinflammatory pathway at the microelectrode-tissue interface in WT mice to investigate the differential expression of genes at chronic time points (4WK, 8WK, and 16WK) post-surgery. We aimed to identify persistently or increasingly differentially expressed genes that may hinder microelectrode integration or offer protective healing to the brain to improve the chronic recording performance of implanted intracortical microelectrodes.

We have found that the gene expression in the neuroinflammatory pathway post-surgery is stable between 4WK to 16WK post-surgery. Overall, 26 out of the 826 genes were identified to be upregulated and only 2 to be downregulated at any point in the study. Of the 28 differentially expressed genes, 68% (19) showed upregulation at all three time points investigated in this study. The stability of gene expression over time points considered to be more chronic found in this study is in contrast with previous studies at acute time points (using the same experimental methods) [63,68], which showed a dynamic upregulation of genes, peaking at 24-72 hours post-surgery. The highest upregulated genes identified in this study are *C3, C4a, Cd36, Cle7a, Gfap, Lilrb4, Mmp12, Serpina3n*, and *Spp1. C3* is a significant component of the complement system and was just one of four genes from the complement system that we found to be differentially expressed in this study. Therefore, *C3,* and more broadly, the complement system, may be strong candidates for therapeutic or gene inhibition studies to improve the integration of intracortical microelectrode and, eventually, their chronic recording performance. While three genes associated with the extracellular matrix were differentially expressed in this study, methods to manipulate extracellular matrix composition to facilitate microelectrode performance are more complex. However, five genes associated with cell surface receptors were differentially expressed in this study. The facilitation of cell-material interactions through various approaches has been shown to mitigate adherent cell density, morphology, proliferation, and function. It has been a popular strategy of the biomaterials community to improve biocompatibility for decades [123–127]. Therefore, the receptor pathways identified here also represent a target of interest for various approaches to mitigate their expression or ability to participate in the neuroinflammatory response to intracortical microelectrode implantation. Moving forward, the genes identified here in either the complement cascade or to be involved in receptor-mediated neuroinflammatory processes will be among the first we continue to explore.

One limitation of our research is that we inserted nonfunctioning probes in the brain to approximate tissue reaction to recording microelectrodes. While we can study the changes in gene expression at the microelectrode-tissue interface, we cannot directly correlate the tissue response to recording signal quality. Future studies using functioning microelectrodes will be able to better correlate the relationship between gene expression and the recording performance of intracortical microelectrodes. Another limitation is that the bulk analysis using tissue extracted manually by biopsy punch is less accurate than that of laser microdissection or spatial proteomics. While we visually check every tissue biopsied to ensure that the site of the implant is as close to the center as possible, even slight imprecision in the centering of the implantation site would lead to the measurement of gene expression beyond a 500 μm radius of implantation site that may dilute the changes in gene expression at the implantation site and alter our results. Furthermore, even when the implantation site is located accurately in the biopsy center, the tissue further away from the implantation site is represented more due to a larger surface area, diluting the difference in gene expression within the tissue closer to implantation. One benefit is that the increased tissue leads to higher coverage of genes expressed; lower expressing genes are not easily missed. In addition, genes identified as differentially expressed using this method would likely exhibit even more differential expression closer to the implantation site.

Finally, it is essential to discuss that the current study could have been more extensive in spatial resolution and cell-specificity of gene expression. The study is also limited to gene expression. We are following up on this study with an in-depth investigation of the cell-specific and spatially resolved analysis of neuroinflammatory pathways with proteomic panels to complement the current research.

No matter the specific tools used, investigating gene expression at the microelectrode-tissue interface is valuable for studying the molecular process in response to microelectrode implantation for BMI applications. This tool should be applied in future studies of tissue response to different microelectrodes, comparing the effects of materials, size, shape, and flexibility on the gene expression and correlating with recording performance.

Author contributions

JRC contributed to the conception and design of the work. SS contributed to the methodology, software analysis, validation, formal analysis, investigation, and data curation. ERC guided the statistical analysis of the work. LD assisted in the validation of the analysis. SS wrote the original draft and figures preparation as well as the review and editing along with JRC. JRC provided the funding and resources to conduct the study.

Disclosures

The contents do not represent the views of the U.S. Department of Veterans Affairs, the National Institutes of Health, or the United States Government.

Declaration of Competing Interest

The authors declare that they have no known competing financial interests or personal relationships that could have appeared to influence the work reported in this paper.

Acknowledgments

The authors acknowledge Dr. Hillary Bedell for completing the acute study that precluded this manuscript. Results generated in

the original manuscript were utilized here to place the chronic results into context. Additionally, we thank BioRender.com as the graphical abstract was Created with BioRender.com.

Funding

This study was supported in part by Merit Review Award, I01RX002611 (Capadona), and Senior Research Career Scientist Award, IK6RX003077 (Capadona), from the United States (US) Department of Veterans Affairs Rehabilitation Research and Development Service. Additionally, this work was also supported in part by the National Institute of Health, National Institute of Neurological Disorders and Stroke, R01NS110823 (Capadona/Pancrazio), and the National Institute for Biomedical Imaging and Bioengineering, T32EB004314 (Capadona/Kirsch).

References

[1] D.H. Hubel, Tungsten microelectrode for recording from single units, Science 125 (3247) (1957) 549–550.
[2] N. Fatima, A. Shuaib, M. Saqqur, Intra-cortical brain-machine interfaces for controlling upper-limb powered muscle and robotic systems in spinal cord injury, Clin. Neurol. Neurosurg. 196 (2020) 106069.
[3] Z.T. Irwin, K.E. Schroeder, P.P. Vu, A.J. Bullard, D.M. Tat, C.S. Nu, A. Vaskov, S.R. Nason, D.E. Thompson, J.N. Bentley, P.G. Patil, C.A. Chestek, Neural control of finger movement via intracortical brain–machine interface, J. Neural Eng. 14 (6) (2017) 066004.
[4] C. Pandarinath, P. Nuyujukian, C.H. Blabe, B.L. Sorice, J. Saab, F.R. Willett, L.R. Hochberg, K.V. Shenoy, J.M. Henderson, High performance communication by people with paralysis using an intracortical brain-computer interface, eLife 6 (2017) e18554.
[5] A.C. Paulk, Y. Kfir, A.R. Khanna, M.L. Mustroph, E.M. Trautmann, D.J. Soper, S.D. Stavisky, M. Welkenhuysen, B. Dutta, K.V. Shenoy, L.R. Hochberg, R.M. Richardson, Z.M. Williams, S.S. Cash, Large-scale neural recordings with single neuron resolution using Neuropixels probes in human cortex, Nat. Neurosci. 25 (2) (2022) 252–263.
[6] A.B. Rapeaux, T.G. Constandinou, Implantable brain machine interfaces: first-in-human studies, technology challenges and trends, Curr. Opin. Biotechnol. 72 (2021) 102–111.
[7] J.D. Simeral, S.P. Kim, M.J. Black, J.P. Donoghue, L.R. Hochberg, Neural control of cursor trajectory and click by a human with tetraplegia 1000 days after implant of an intracortical microelectrode array, J. Neural Eng. 8 (2) (2011) 025027.
[8] F.R. Willett, D.T. Avansino, L.R. Hochberg, J.M. Henderson, K.V. Shenoy, High-performance brain-to-text communication via handwriting, Nature 593 (7858) (2021) 249–254.
[9] M.E. Obien, K. Deligkaris, T. Bullmann, D.J. Bakkum, U. Frey, Revealing neuronal function through microelectrode array recordings, Front. Neurosci. 8 (2014) 423.
[10] D.H. Hubel, T.N. Wiesel, Receptive fields of single neurones in the cat's striate cortex, J. Physiol. 148 (1959) 574–591.
[11] J. Muller, M. Ballini, P. Livi, Y. Chen, M. Radivojevic, A. Shadmani, V. Viswam, I.L. Jones, M. Fiscella, R. Diggelmann, A. Stettler, U. Frey, D.J. Bakkum, A. Hierlemann, High-resolution CMOS MEA platform to study neurons at subcellular, cellular, and network levels, Lab Chip 15 (13) (2015) 2767–2780.
[12] A. Stett, U. Egert, E. Guenther, F. Hofmann, T. Meyer, W. Nisch, H. Haemmerle, Biological application of microelectrode arrays in drug discovery and basic research, Anal. Bioanal. Chem. 377 (3) (2003) 486–495.
[13] T. Proix, M. Aghagolzadeh, J.R. Madsen, R. Cosgrove, E. Eskandar, L.R. Hochberg, S.S. Cash, W. Truccolo, Intracortical neural activity distal to seizure-onset-areas predicts human focal seizures, PLoS One 14 (7) (2019) e0211847.
[14] C. Heelan, J. Lee, R. O'Shea, L. Lynch, D.M. Brandman, W. Truccolo, A.V. Nurmikko, Decoding speech from spike-based neural population recordings in secondary auditory cortex of non-human primates, Commun. Biol. 2 (1) (2019) 466.
[15] A.B. Ajiboye, F.R. Willett, D.R. Young, W.D. Memberg, B.A. Murphy, J.P. Miller, B.L. Walter, J.A. Sweet, H.A. Hoyen, M.W. Keith, P.H. Peckham, J.D. Simeral, J.P. Donoghue, L.R. Hochberg, R.F. Kirsch, Restoration of reaching and grasping movements through brain-controlled muscle stimulation in a person with tetraplegia: a proof-of-concept demonstration, Lancet 389 (10081) (2017) 1821–1830.
[16] B. Jarosiewicz, A.A. Sarma, D. Bacher, N.Y. Masse, J.D. Simeral, B. Sorice, E.M. Oakley, C. Blabe, C. Pandarinath, V. Gilja, S.S. Cash, E.N. Eskandar, G. Friehs, J.M. Henderson, K.V. Shenoy, J.P. Donoghue, L.R. Hochberg, Virtual typing by people with tetraplegia using a self-calibrating intracortical brain–computer interface, Sci. Transl. Med. 7 (313) (2015) 313ra179.
[17] L.R. Hochberg, M.D. Serruya, G.M. Friehs, J.A. Mukand, M. Saleh, A.H. Caplan, A. Branner, D. Chen, R.D. Penn, J.P. Donoghue, Neuronal ensemble control of prosthetic devices by a human with tetraplegia, Nature 442 (7099) (2006) 164–171.
[18] L.R. Hochberg, J.P. Donoghue, Sensors for brain-computer interfaces, IEEE Eng. Med. Biol. Mag. 25 (5) (2006) 32–38.
[19] A. Khorasani, N. Heydari Beni, V. Shalchyan, M.R. Daliri, Continuous force decoding from local field potentials of the primary motor cortex in freely moving rats, Sci. Rep. 6 (1) (2016) 35238.
[20] Y.S. Park, G.R. Cosgrove, J.R. Madsen, E.N. Eskandar, L.R. Hochberg, S.S. Cash, W. Truccolo, Early detection of human epileptic seizures based on intracortical microelectrode array signals, IEEE Trans. Biomed. Eng. 67 (3) (2020) 817–831.
[21] K.E. Schroeder, C.A. Chestek, Intracortical brain-machine interfaces advance sensorimotor neuroscience, Front. Neurosci. 10 (2016).
[22] T.D.Y. Kozai, A.S. Jaquins-Gerstl, A.L. Vazquez, A.C. Michael, X.T. Cui, Brain tissue responses to neural implants impact signal sensitivity and intervention strategies, ACS Chem. Neurosci. 6 (1) (2015) 48–67.
[23] N.F. Nolta, M.B. Christensen, P.D. Crane, J.L. Skousen, P.A. Tresco, BBB leakage, astrogliosis, and tissue loss correlate with silicon microelectrode array recording performance, Biomaterials 53 (2015) 753–762.
[24] K.A. Potter, A.C. Buck, W.K. Self, J.R. Capadona, Stab injury and device implantation within the brain results in inversely multiphasic neuroinflammatory and neurodegenerative responses, J. Neural Eng. 9 (4) (2012) 046020.
[25] T. Saxena, L. Karumbaiah, E.A. Gaupp, R. Patkar, K. Patil, M. Betancur, G.B. Stanley, R.V. Bellamkonda, The impact of chronic blood–brain barrier breach on intracortical electrode function, Biomaterials 34 (20) (2013) 4703–4713.
[26] A.J. Shoffstall, J.E. Paiz, D.M. Miller, G.M. Rial, M.T. Willis, D.M. Menendez, S.R. Hostler, J.R. Capadona, Potential for thermal damage to the blood-brain barrier during craniotomy: implications for intracortical recording microelectrodes, J. Neural Eng. 15 (3) (2018) 034001.
[27] C.S. Bjornsson, S.J. Oh, Y.A. Al-Kofahi, Y.J. Lim, K.L. Smith, J.N. Turner, S. De, B. Roysam, W. Shain, S.J. Kim, Effects of insertion conditions on tissue strain and vascular damage during neuroprosthetic device insertion, J. Neural Eng. 3 (3) (2006) 196–207.
[28] B. Money, A. Hess-Dunning, P. Gloth, J.R. Capadona, C. Weder, Mechanically adaptive implants fabricated with poly(2-hydroxy¬ethyl methacrylate)-based negative photoresists, J. Mater. Chem. B (2020).
[29] H.W. Bedell, S. Song, X. Li, E. Molinich, S. Lin, W.E. Voit, J.J. Pancrazio, J.R. Capadona, Understanding the effects of both CD14-meditated innate immunity and device/tissue mechanical mismatch in the neuroinflammatory response to intracortical microelectrodes, Front. Neurosci. 12 (2018) 772.
[30] J.K. Nguyen, M. Jorfi, K.L. Buchanan, D.J. Park, E.J. Foster, D.J. Tyler, S.J. Rowan, C. Weder, J.R. Capadona, Influence of resveratrol release on the tissue response to mechanically adaptive cortical implants, Acta Biomater. 29 (2016) 81–93.
[31] A. Sridharan, J.K. Nguyen, J.R. Capadona, J. Muthuswamy, Compliant intracortical implants reduce strains and strain rates in brain tissue in vivo, J. Neural Eng. 12 (3) (2015) 036002.
[32] J.K. Nguyen, D.J. Park, J.L. Skousen, A. Hess-Dunning, D.J. Tyler, S.J. Rowan, C. Weder, J.R. Capadona, Mechanically-compliant intracortical implants reduce the neuroinflammatory response, J. Neural Eng. 11 (2014) 056014.
[33] J.P. Harris, J.R. Capadona, R.H. Miller, B.C. Healy, K. Shanmuganathan, S.J. Rowan, C. Weder, D.J. Tyler, Mechanically adaptive intracortical implants improve the proximity of neuronal cell bodies, J. Neural Eng. 8 (6) (2011) 066011.
[34] D.M. Simon, H. Charkhkar, C. St John, S. Rajendran, T. Kang, R. Reit, D. Arreaga-Salas, D.G. McHail, G.L. Knaack, A. Sloan, D. Grasse, T.C. Dumas, R.L. Rennaker, J.J. Pancrazio, W.E. Voit, Design and demonstration of an intracortical probe technology with tunable modulus, J. Biomed. Mater. Res. A 105 (1) (2017) 159–168.
[35] T. Ware, D. Simon, D.E. Arreaga-Salas, J. Reeder, R. Rennaker, E.W. Keefer, W. Voit, Fabrication of responsive, softening neural interfaces, Adv. Funct. Mater. 22 (16) (2012) 3470–3479.
[36] E.J. Welle, P.R. Patel, J.E. Woods, A. Petrossians, E.Della Valle, A. Vega-Medina, J.M. Richie, D. Cai, J.D. Weiland, C.A. Chestek, Ultra-small carbon fiber electrode recording site optimization and improved in vivo chronic recording yield, J. Neural Eng. 17 (2) (2020) 026037.
[37] E.S. Ereifej, G. Rial, J.K. Hermann, C.S. Smith, S. Meade, J. Rayyan, K. Chen, H. Feng, J.R. Capadona, Implantation of neural probes in the brain elicits oxidative stress, Front. Bioeng. Biotechnol. 6 (9) (2018) 1–12.
[38] K.A. Potter, A.C. Buck, W.K. Self, M.E. Callanan, S. Sunil, J.R. Capadona, The effect of resveratrol on neurodegeneration and blood brain barrier stability surrounding intracortical microelectrodes, Biomaterials 34 (29) (2013) 7001–7015.
[39] K.A. Potter, M. Jorfi, K.T. Householder, E.J. Foster, C. Weder, J.R. Capadona, Curcumin-releasing mechanically-adaptive intracortical implants improve the proximal neuronal density and blood-brain barrier stability, Acta Biomater. 10 (5) (2014) 2209–2222.
[40] K.A. Potter-Baker, J.R. Capadona, Reducing the "stress": antioxidative therapeutic and material approaches may prevent intracortical microelectrode failure, ACS Macro Lett. (2015) 275–279.
[41] K.A. Potter-Baker, J.K. Nguyen, K.M. Kovach, M.M. Gitomer, T.W. Srail, W.G. Stewart, J.L. Skousen, J.R. Capadona, Development of superoxide dismutase mimetic surfaces to reduce accumulation of reactive oxygen species surrounding intracortical microelectrodes, J. Mater. Chem. B 2 (2014) 2248–2258.
[42] K.A. Potter-Baker, W.G. Stewart, W.H. Tomaszewski, C.T. Wong, W.D. Meador, N.P. Ziats, J.R. Capadona, Implications of chronic daily anti-oxidant adminis-

tration on the inflammatory response to intracortical microelectrodes, J. Neural Eng. 12 (4) (2015) 046002.
[43] C. Bennett, F. Mohammed, A. Alvarez-Ciara, M.A. Nguyen, W.D. Dietrich, S.M. Rajguru, W.J. Streit, A. Prasad, Neuroinflammation, oxidative stress, and blood-brain barrier (BBB) disruption in acute Utah electrode array implants and the effect of deferoxamine as an iron chelator on acute foreign body response, Biomaterials 188 (2019) 144–159.
[44] A.G. Hernandez-Reynoso, O.K. Krebs, B. Sturgill, G.F. Hoeferlin, R. Radhakrishna, T.J. Smith, J. Zhang, G. Mittal, T.T.D. Thai, M.S. Desai, S.F. Cogan, J.J. Pancrazio, J.R. Capadona, The effect of a superoxide dismutase mimetic coating on the acute and sub-chronic recording performance of planar silicon intracortical microelectrode arrays, Biomaterials (2022) Under Review.
[45] L. Spataro, J. Dilgen, S. Retterer, A.J. Spence, M. Isaacson, J.N. Turner, W. Shain, Dexamethasone treatment reduces astroglia responses to inserted neuroprosthetic devices in rat neocortex, Exp. Neurol. 194 (2) (2005) 289–300.
[46] R.L. Rennaker, J. Miller, H. Tang, D.A. Wilson, Minocycline increases quality and longevity of chronic neural recordings, J. Neural Eng. 4 (2) (2007) L1–L5.
[47] J.K. Hermann, M. Ravikumar, A.J. Shoffstall, E.S. Ereifej, K.M. Kovach, J. Chang, A. Soffer, C. Wong, V. Srivastava, P. Smith, G. Protasiewicz, J. Jiang, S.M. Selkirk, R.H. Miller, S. Sidik, N.P. Ziats, D.M. Taylor, J.R. Capadona, Inhibition of the cluster of differentiation 14 innate immunity pathway with IAXO-101 improves chronic microelectrode performance, J. Neural Eng. 15 (2) (2018) 025002.
[48] Y. Zhong, R.V. Bellamkonda, Dexamethasone-coated neural probes elicit attenuated inflammatory response and neuronal loss compared to uncoated neural probes, Brain Res. 1148 (2007) 15–27.
[49] W. He, G.C. McConnell, R.V. Bellamkonda, Nanoscale laminin coating modulates cortical scarring response around implanted silicon microelectrode arrays, J. Neural Eng. 3 (4) (2006) 316–326.
[50] A. Golabchi, B. Wu, X. Li, D.L. Carlisle, T.D.Y. Kozai, R.M. Friedlander, X.T. Cui, Melatonin improves quality and longevity of chronic neural recording, Biomaterials 180 (2018) 225–239.
[51] E.K. Purcell, D.E. Thompson, K.A. Ludwig, D.R. Kipke, Flavopiridol reduces the impedance of neural prostheses in vivo without affecting recording quality, J. Neurosci. Methods 183 (2) (2009) 149–157.
[52] T.D. Kozai, X. Li, L.M. Bodily, E.M. Caparosa, G.A. Zenonos, D.L. Carlisle, R.M. Friedlander, X.T. Cui, Effects of caspase-1 knockout on chronic neural recording quality and longevity: insight into cellular and molecular mechanisms of the reactive tissue response, Biomaterials 35 (36) (2014) 9620–9634.
[53] R.S. Oakes, M.D. Polei, J.L. Skousen, P.A. Tresco, An astrocyte derived extracellular matrix coating reduces astrogliosis surrounding chronically implanted microelectrode arrays in rat cortex, Biomaterials 154 (2018) 1–11.
[54] A. Golabchi, K.M. Woeppel, X. Li, C.F. Lagenaur, X.T. Cui, Neuroadhesive protein coating improves the chronic performance of neuroelectronics in mouse brain, Biosens. Bioelectron. 155 (2020) 112096.
[55] J. Curran, J. Lo, V. Leung, K. Brown, K.L. Schwartz, N. Daneman, G. Garber, J.H.C. Wu, B.J. Langford, Estimating daily antibiotic harms: an umbrella review with individual study meta-analysis, Clin. Microbiol. Infect. 28 (4) (2022) 479–490.
[56] Y. Heianza, W. Ma, X. Li, Y. Cao, A.T. Chan, E.B. Rimm, F.B. Hu, K.M. Rexrode, J.E. Manson, L. Qi, Duration and life-stage of antibiotic use and risks of all-cause and cause-specific mortality: prospective cohort study, Circ. Res. 126 (3) (2020) 364–373.
[57] R. Kaki, M. Elligsen, S. Walker, A. Simor, L. Palmay, N. Daneman, Impact of antimicrobial stewardship in critical care: a systematic review, J. Antimicrob. Chemother. 66 (6) (2011) 1223–1230.
[58] A.L. Buchman, Side effects of corticosteroid therapy, J. Clin. Gastroenterol. 33 (4) (2001) 289–294.
[59] B. Brommer, O. Engel, M.A. Kopp, R. Watzlawick, S. Muller, H. Pruss, Y. Chen, M.J. DeVivo, F.W. Finkenstaedt, U. Dirnagl, T. Liebscher, A. Meisel, J.M. Schwab, Spinal cord injury-induced immune deficiency syndrome enhances infection susceptibility dependent on lesion level, Brain 139 (Pt 3) (2016) 692–707.
[60] T. Riegger, S. Conrad, H.J. Schluesener, H.P. Kaps, A. Badke, C. Baron, J. Gerstein, K. Dietz, M. Abdizahdeh, J.M. Schwab, Immune depression syndrome following human spinal cord injury (SCI): a pilot study, Neuroscience 158 (3) (2009) 1194–1199.
[61] K.A. Rodgers, K.A. Kigerl, J.M. Schwab, P.G. Popovich, Immune dysfunction after spinal cord injury - a review of autonomic and neuroendocrine mechanisms, Curr. Opin. Pharmacol. 64 (2022) 102230.
[62] Y. Zhang, Z. Guan, B. Reader, T. Shawler, S. Mandrekar-Colucci, K. Huang, Z. Weil, A. Bratasz, J. Wells, N.D. Powell, J.F. Sheridan, C.C. Whitacre, A.G. Rabchevsky, M.S. Nash, P.G. Popovich, Autonomic dysreflexia causes chronic immune suppression after spinal cord injury, J. Neurosci. 33 (32) (2013) 12970–12981.
[63] H.W. Bedell, N.J. Schaub, J.R. Capadona, E.S. Ereifej, Differential expression of genes involved in the acute innate immune response to intracortical microelectrodes, Acta Biomater. 102 (2020) 205–219.
[64] J.D. Falcone, S.L. Carroll, T. Saxena, D. Mandavia, A. Clark, V. Yarabarla, R.V. Bellamkonda, Correlation of mRNA expression and signal variability in chronic intracortical electrodes, Front. Bioeng. Biotechnol. 6 (2018) 26.
[65] C.H. Thompson, A. Saxena, N. Heelan, J. Salatino, E.K. Purcell, Spatiotemporal patterns of gene expression around implanted silicon electrode arrays, J. Neural Eng. 18 (4) (2021).
[66] K. Joseph, M. Kirsch, M. Johnston, C. Munkel, T. Stieglitz, C.A. Haas, U.G. Hofmann, Transcriptional characterization of the glial response due to chronic neural implantation of flexible microprobes, Biomaterials 279 (2021) 121230.
[67] E.S. Ereifej, G.M. Rial, J.K. Hermann, C.S. Smith, S.M. Meade, J.M. Rayyan, K. Chen, H. Feng, J.R. Capadona, Implantation of neural probes in the brain elicits oxidative stress, Front. Bioeng. Biotechnol. 6 (2018) 9.
[68] S. Song, B. Regan, E.S. Ereifej, E.R. Chan, J.R. Capadona, Neuroinflammatory gene expression analysis reveals pathways of interest as potential targets to improve the recording performance of intracortical microelectrodes, Cells 11 (15) (2022).
[69] H.W.B.S. Song, B.J. Regan, E.S. Ereifej, R. Chan, J.R. Capadona, Neuroinflammatory gene expression analysis reveals pathways of interest as potential targets to improve the recording performance of intracortical microelectrodes, Cells 11 (15) (2022) 2348.
[70] D.M.M.G.F. Hoeferlin, O.K. Krebs, J.R. Capadona, A.J. Shoffstall, Assessment of thermal damage from robot-drilled craniotomy for cranial window surgery in mice, J. Visualized Exp. : Jove 189 (2022).
[71] E.S. Ereifej, C.S. Smith, S.M. Meade, K. Chen, H. Feng, J.R. Capadona, The neuroinflammatory response to nanopatterning parallel grooves into the surface structure of intracortical microelectrodes, Adv. Funct. Mater. 28 (12) (2018) 1704420.
[72] M. Ravikumar, D.J. Hageman, W.H. Tomaszewski, G.M. Chandra, J.L. Skousen, J.R. Capadona, The effect of residual endotoxin contamination on the neuroinflammatory response to sterilized intracortical microelectrodes, J. Mater. Chem. B 2 (2014) 2517–2529.
[73] M. Ravikumar, S. Sunil, J. Black, D. Barkauskas, A.Y. Haung, R.H. Miller, S.M. Selkirk, J.R. Capadona, The roles of blood-derived macrophages and resident microglia in the neuroinflammatory response to implanted intracortical microelectrodes, Biomaterials S0142-9612 (35) (2014) 8049–8064.
[74] B.J. Gates, T.T. Nguyen, S.M. Setter, N.M. Davies, Meloxicam: a reappraisal of pharmacokinetics, efficacy and safety, Expert Opin. Pharmacother. 6 (12) (2005) 2117–2140.
[75] G. Hoeferlin, D. Menendez, O. Krebs, J. Capadona, A. Shoffstall, Assessment of thermal damage from robot-drilled craniotomy for cranial window surgery in mice, J. Visualized Exp. : Jove 189 (2022).
[76] F. Orsini, D. De Blasio, R. Zangari, E.R. Zanier, M.G. De Simoni, Versatility of the complement system in neuroinflammation, neurodegeneration and brain homeostasis, Front. Cell Neurosci. 8 (2014) 380.
[77] I. Song, A. Dityatev, Crosstalk between glia, extracellular matrix and neurons, Brain Res. Bull. 136 (2018) 101–108.
[78] D.G. Jang, H.J. Sim, E.K. Song, T. Kwon, T.J. Park, Extracellular matrixes and neuroinflammation, BMB Rep. 53 (10) (2020) 491–499.
[79] A. Suttkus, M. Morawski, T. Arendt, Protective properties of neural extracellular matrix, Mol. Neurobiol. 53 (1) (2016) 73–82.
[80] D.R. Mathern, P.S. Heeger, Molecules great and small: the complement system, Clin. J. Am. Soc. Nephrol. 10 (9) (2015) 1636–1650.
[81] A. Doni, C. Garlanda, B. Bottazzi, S. Meri, P. Garred, A. Mantovani, Interactions of the humoral pattern recognition molecule PTX3 with the complement system, Immunobiology 217 (11) (2012) 1122–1128.
[82] K. Haapasalo, S. Meri, Regulation of the complement system by pentraxins, Front. Immunol. 10 (2019) 1750.
[83] S.M. Moghimi, A.J. Andersen, D. Ahmadvand, P.P. Wibroe, T.L. Andresen, A.C. Hunter, Material properties in complement activation, Adv. Drug. Deliv. Rev. 63 (12) (2011) 1000–1007.
[84] Y. Arima, M. Toda, H. Iwata, Surface plasmon resonance in monitoring of complement activation on biomaterials, Adv. Drug. Deliv. Rev. 63 (12) (2011) 988–999.
[85] G. Bergseth, J.D. Lambris, T.E. Mollnes, K.T. Lappegard, Artificial surface-induced inflammation relies on complement factor 5: proof from a deficient person, Ann. Thorac. Surg. 91 (2) (2011) 527–533.
[86] B. Nilsson, K.N. Ekdahl, T.E. Mollnes, J.D. Lambris, The role of complement in biomaterial-induced inflammation, Mol. Immunol. 44 (1-3) (2007) 82–94.
[87] L. Tang, L. Liu, H.B. Elwing, Complement activation and inflammation triggered by model biomaterial surfaces, J. Biomed. Mater. Res. 41 (2) (1998) 333–340.
[88] K.N. Ekdahl, J.D. Lambris, H. Elwing, D. Ricklin, P.H. Nilsson, Y. Teramura, I.A. Nicholls, B. Nilsson, Innate immunity activation on biomaterial surfaces: a mechanistic model and coping strategies, Adv. Drug. Deliv. Rev. 63 (12) (2011) 1042–1050.
[89] H. Laronha, J. Caldeira, Structure and function of human matrix metalloproteinases, Cells 9 (5) (2020).
[90] J.N. Hahn, D.K. Kaushik, M.K. Mishra, J. Wang, C. Silva, V.W. Yong, Impact of minocycline on extracellular matrix metalloproteinase inducer, a factor implicated in multiple sclerosis immunopathogenesis, J. Immunol. 197 (10) (2016) 3850–3860.
[91] H. Suzuki, Y. Sugimura, S. Iwama, H. Suzuki, O. Nobuaki, H. Nagasaki, H. Arima, M. Sawada, Y. Oiso, Minocycline prevents osmotic demyelination syndrome by inhibiting the activation of microglia, J. Am. Soc. Nephrol. 21 (12) (2010) 2090–2098.
[92] H.W. Tun, D. Personett, K.A. Baskerville, D.M. Menke, K.A. Jaeckle, P. Kreinest, B. Edenfield, A.C. Zubair, B.P. O'Neill, W.R. Lai, P.J. Park, M. McKinney, Pathway analysis of primary central nervous system lymphoma, Blood 111 (6) (2008) 3200–3210.
[93] H. Yu, X. Liu, Y. Zhong, The effect of osteopontin on microglia, Biomed. Res. Int. 2017 (2017) 1879437.
[94] A. Yim, C. Smith, A.M. Brown, Osteopontin/secreted phosphoprotein-1 harnesses glial-, immune-, and neuronal cell ligand-receptor interactions to sense and regulate acute and chronic neuroinflammation, Immunol. Rev. 311 (1) (2022) 224–233.

[95] Y. Yoo, E. Choi, Y. Kim, Y. Cha, E. Um, Y. Kim, Y. Kim, Y.S. Lee, Therapeutic potential of targeting cathepsin S in pulmonary fibrosis, Biomed. Pharmacother. 145 (2022) 112245.
[96] C. Sousa, A. Golebiewska, S.K. Poovathingal, T. Kaoma, Y. Pires-Afonso, S. Martina, D. Coowar, F. Azuaje, A. Skupin, R. Balling, K. Biber, S.P. Niclou, A. Michelucci, Single-cell transcriptomics reveals distinct inflammation-induced microglia signatures, EMBO Rep. 19 (11) (2018).
[97] V.R. Krishnaswamy, A. Benbenishty, P. Blinder, I. Sagi, Demystifying the extracellular matrix and its proteolytic remodeling in the brain: structural and functional insights, Cell. Mol. Life Sci. 76 (16) (2019) 3229–3248.
[98] M. Morawski, M. Filippov, A. Tzinia, E. Tsilibary, L. Vargova, ECM in brain aging and dementia, Prog. Brain Res. 214 (2014) 207–227.
[99] R. Biran, D.C. Martin, P.A. Tresco, Neuronal cell loss accompanies the brain tissue response to chronically implanted silicon microelectrode arrays, Exp. Neurol. 195 (1) (2005) 115–126.
[100] S.M. Gutowski, K.L. Templeman, A.B. South, J.C. Gaulding, J.T. Shoemaker, M.C. LaPlaca, R.V. Bellamkonda, L.A. Lyon, A.J. Garcia, Host response to microgel coatings on neural electrodes implanted in the brain, J. Biomed. Mater. Res. A 102 (5) (2014) 1486–1499.
[101] G.C. McConnell, H.D. Rees, A.I. Levey, C.-A. Gutekunst, R.E. Gross, R.V. Bellamkonda, Implanted neural electrodes cause chronic, local inflammation that is correlated with local neurodegeneration, J. Neural Eng. 6 (5) (2009) 056003.
[102] K. Chen, S.M. Wellman, Y. Yaxiaer, J.R. Eles, T.D. Kozai, In vivo spatiotemporal patterns of oligodendrocyte and myelin damage at the neural electrode interface, Biomaterials 268 (2021) 120526.
[103] N.J. Michelson, A.L. Vazquez, J.R. Eles, J.W. Salatino, E.K. Purcell, J.J. Williams, X.T. Cui, T.D.Y. Kozai, Multi-scale, multi-modal analysis uncovers complex relationship at the brain tissue-implant neural interface: new emphasis on the biological interface, J. Neural Eng. 15 (3) (2018) 033001.
[104] L. Chavez-Sanchez, M.G. Garza-Reyes, J.E. Espinosa-Luna, K. Chavez-Rueda, M.V. Legorreta-Haquet, F. Blanco-Favela, The role of TLR2, TLR4 and CD36 in macrophage activation and foam cell formation in response to oxLDL in humans, Hum. Immunol. 75 (4) (2014) 322–329.
[105] Y.M. Park, CD36, a scavenger receptor implicated in atherosclerosis, Exp. Mol. Med. 46 (6) (2014) e99.
[106] R.L. Silverstein, M. Febbraio, CD36, a scavenger receptor involved in immunity, metabolism, angiogenesis, and behavior, Sci. Signal 2 (72) (2009) re3.
[107] C.M. Niculite, A.M. Enciu, M.E. Hinescu, CD 36: focus on epigenetic and post–transcriptional regulation, Front. Genet. 10 (2019) 680.
[108] N. Kalia, J. Singh, M. Kaur, The role of dectin-1 in health and disease, Immunobiology 226 (2) (2021) 152071.
[109] M.E. Deerhake, K. Danzaki, M. Inoue, E.D. Cardakli, T. Nonaka, N. Aggarwal, W.E. Barclay, R.R. Ji, M.L. Shinohara, Dectin-1 limits autoimmune neuroinflammation and promotes myeloid cell-astrocyte crosstalk via Card9-independent expression of Oncostatin M, Immunity 54 (3) (2021) 484-498 e8.
[110] M.E. Deerhake, M.L. Shinohara, Emerging roles of Dectin-1 in noninfectious settings and in the CNS, Trends Immunol. 42 (10) (2021) 891–903.
[111] L.A. Hohsfield, A.R. Najafi, Y. Ghorbanian, N. Soni, E.E. Hingco, S.J. Kim, A.D. Jue, V. Swarup, M.A. Inlay, K.N. Green, Effects of long-term and brain-wide colonization of peripheral bone marrow-derived myeloid cells in the CNS, J. Neuroinflamm. 17 (1) (2020) 279.
[112] M. Al-Ani, N.M. Elemam, I.Y. Hachim, T.K. Raju, J.S. Muhammad, M.Y. Hachim, R. Bendardaf, A.A. Maghazachi, Molecular examination of differentially expressed genes in the brains of experimental autoimmune encephalomyelitis mice post herceptin treatment, J. Inflamm. Res. 14 (2021) 2601–2617.
[113] P. Chauhan, S. Hu, W.S. Sheng, S. Prasad, J.R. Lokensgard, Modulation of microglial cell Fcgamma receptor expression following viral brain infection, Sci. Rep. 7 (2017) 41889.
[114] J.M. Anderson, A. Rodriguez, D.T. Chang, Foreign body reaction to biomaterials, Semin. Immunol. 20 (2008) 86–100.
[115] S.M. Gutowski, J.T. Shoemaker, K.L. Templeman, Y. Wei, R.A. Latour Jr., R.V. Bellamkonda, M.C. LaPlaca, A.J. Garcia, Protease-degradable PEG–maleimide coating with on-demand release of IL-1Ra to improve tissue response to neural electrodes, Biomaterials 44 (2015) 55–70.
[116] Y. Zhong, R.V. Bellamkonda, Controlled release of anti-inflammatory agent α-MSH from neural implants, J. Controlled Release 106 (3) (2005) 309–318.
[117] L. Tarassishin, H.S. Suh, S.C. Lee, LPS and IL-1 differentially activate mouse and human astrocytes: role of CD14, Glia 62 (6) (2014) 999–1013.
[118] Z.M. Wang, C. Liu, Y.Y. Wang, Y.S. Deng, X.C. He, H.Z. Du, C.M. Liu, Z.Q. Teng, SerpinA3N deficiency deteriorates impairments of learning and memory in mice following hippocampal stab injury, Cell Death Discov. 6 (1) (2020) 88.
[119] J.L. Zamanian, L. Xu, L.C. Foo, N. Nouri, L. Zhou, R.G. Giffard, B.A. Barres, Genomic analysis of reactive astrogliosis, J. Neurosci. 32 (18) (2012) 6391–6410.
[120] M. Zattoni, M. Mearelli, S. Vanni, A. Colini Baldeschi, T.H. Tran, C. Ferracin, M. Catania, F. Moda, G. Di Fede, G. Giaccone, F. Tagliavini, G. Zanusso, J.W. Ironside, I. Ferrer, G. Legname, Serpin signatures in prion and Alzheimer's diseases, Mol. Neurobiol. 59 (6) (2022) 3778–3799.
[121] Y. Zhang, Q. Chen, D. Chen, W. Zhao, H. Wang, M. Yang, Z. Xiang, H. Yuan, SerpinA3N attenuates ischemic stroke injury by reducing apoptosis and neuroinflammation, CNS Neurosci. Ther. 28 (4) (2022) 566–579.
[122] Y. Xi, M. Liu, S. Xu, H. Hong, M. Chen, L. Tian, J. Xie, P. Deng, C. Zhou, L. Zhang, M. He, C. Chen, Y. Lu, R.J. Reiter, Z. Yu, H. Pi, Z. Zhou, Inhibition of SERPINA3N-dependent neuroinflammation is essential for melatonin to ameliorate trimethyltin chloride-induced neurotoxicity, J. Pineal Res. 67 (3) (2019) e12596.
[123] T.A. Petrie, J.R. Capadona, C.D. Reyes, A.J. Garcia, Integrin specificity and enhanced cellular activities associated with surfaces presenting a recombinant fibronectin fragment compared to RGD supports, Biomaterials 27 (2006) 5459–5470.
[124] T.A. Petrie, J.E. Raynor, C.D. Reyes, K.L. Burns, D.M. Collard, A.J. García, The effect of integrin-specific bioactive coatings on tissue healing and implant osseointegration, Biomaterials 29 (19) (2008) 2849–2857.
[125] J.E. Raynor, J.R. Capadona, D.M. Collard, T.A. Petrie, A.J. Garcia, Polymer brushes and self-assembled monolayers: versatile platforms to control cell adhesion to biomaterials (Review), Biointerphases 4 (2) (2009) FA3–F16.
[126] A.R. Prachi Dhavalikar, Z. Lan, D. Jenkins, M. Chwatko, K. Salhadar, A. Jose, R. Kar, E. Shoga, A. Kannapiran, E. Cosgriff-Hernandez, Review of integrin-targeting biomaterials in tissue engineering, 9(23) (2020) 2000795.
[127] M.C. Tate, A.J. Garcia, B.G. Keselowsky, M.A. Schumm, D.R. Archer, M.C. LaPlaca, Specific beta1 integrins mediate adhesion, migration, and differentiation of neural progenitors derived from the embryonic striatum, Mol. Cell. Neurosci. 27 (1) (2004) 22–31.